Cholesterol-induced conformational changes in the oxytocin receptor

Sabine Muth, Anja Fries, Gerald Gimpl

Cholesterol-induced conformational changes in the oxytocin receptor

Sabine Muth, Anja Fries, and Gerald Gimpl*

Institute of Pharmacy and Biochemistry, Department of Biochemistry, Gutenberg-University Mainz, Johann-Joachim Becherweg 30, D-55128 Mainz, Germany

Running Title: Cholesterol-receptor interaction

***Correspondence**:
Institute of Pharmacy and Biochemistry, Department of Biochemistry, Gutenberg-University Mainz, Johann-Joachim Becherweg 30, 55128 Mainz, Germany
Fax: +49 6131 3925348
Tel: +49 6131 3920208
E-mail: gimpl@uni-mainz.de

Abbreviations:
BTB, bungarotoxin binding site
DChol, 6-dansyl-cholestanol
EGFP, enhanced green fluorescent protein
FRET, fluorescence resonance energy transfer
GPCR, G protein coupled receptor
OTAN, oxytocin antagonist
OTR, oxytocin receptor
TEMPO, 2,2,6,6-tetramethylpiperidine-1-oxyl

Keywords: cholesterol; oxytocin receptor; bungarotoxin binding site;

Summary

Recent studies suggest that cholesterol binding is widespread among G protein coupled receptors (GPCRs). Here, we analyzed putative cholesterol-induced changes in the oxytocin receptor, a prototype of cholesterol-interacting GPCRs. For this purpose, we have created recombinant oxytocin receptors that are able to bind two small-sized fluorescence-labeled ligands simultaneously. An oxytocin receptor antagonist was chosen as one of the ligands. To create a second ligand binding site, a small-sized α-bungarotoxin binding site was inserted at the N-terminus or within the third extracellular loop of the oxytocin receptor. All receptor constructs were functionally active and bound both ligands with high-affinity in the nanomolar range. Measurements of the quenching behavior, fluorescence anisotropy and energy transfer of both receptor bound ligands were performed to monitor receptor states at varying cholesterol. The quenching studies suggested no major changes in the molecular environment of the fluorophores in response to cholesterol. The fluorescence anisotropy data indicated that cholesterol affects the dynamics or orientation of the antagonist. The energy transfer efficiency between both ligands clearly increased with increasing cholesterol. Overall, cholesterol induced both a changed orientation and a decreased distance of the receptor bound ligands suggesting a more compact receptor state in association with cholesterol.

Introduction

G protein coupled receptors (GPCRs) comprise the largest and most diverse receptor superfamily involved in signal transduction across membranes [31]. Due to their integration into the membrane bilayer with seven transmembrane helices, GPCRs are in close contact to membrane lipids. Among those lipids, cholesterol is one of the most abundant in the plasma membrane of eukaryotic cells. Cholesterol is a multifunctional lipid. It regulates the fluidity and the phase behavior of the membrane bilayer, serves as precursor of steroid hormones and some vitamins, is essentially involved in the formation of lateral membrane microdomains (e.g. lipid rafts, caveolae) [24,35], and plays a crucial role in the function and organization of membrane proteins, e.g. receptors and ion channels [5,22,29].

Direct GPCR-cholesterol interactions have been suggested for the oxytocin, galanin, and serotonin$_{1A}$ receptors [10,27,28]. To fulfill their function in signal transduction, GPCRs require conformational flexibility. There is some evidence that cholesterol is able to stabilize the conformation of receptors, e.g. the β_2-adrenergic receptor [16,40] and the oxytocin receptor [11]. Recent structural data supported the stabilizing role of cholesterol for the conformation of GPCRs [6,16]. Based on homology, a so-called ´cholesterol consensus motif` has been defined that is found in more than 40 class A GPCRs including the cholesterol-dependent oxytocin receptor [16]. Thus, cholesterol binding is rather widespread among the GPCRs and the oxytocin receptor can be regarded as a prototype of these cholesterol-interacting receptors.

Here, we asked whether cholesterol-dependent changes of receptor conformations are detectable. For this purpose, the fluorescence properties of specifically bound ligands were exploited to report on the molecular behavior and environment of the oxytocin receptor. Specifically, the goal was to find an appropriate combination of two ligands that are able to bind simultaneously to one receptor molecule. Under certain conditions,

changes of the relative distance or orientation of the bound ligands (e.g. measurable by FRET) will reflect structural changes of the receptor. The two ligands required for this study should be as small as possible and possess non-overlapping binding sites at the receptor molecule. An oxytocin receptor antagonist was chosen as one of the receptor ligands. Other known high-affinity ligands of the oxytocin receptor are expected to overlap (at least partially) with the antagonist receptor binding site and are therefore excluded as a potential further receptor binding partner. In order to create a second ligand-specific binding site at the oxytocin receptor, we introduced a small-sized epitope comprising 13 amino acids (WRYYESSLEPYPD) at different positions of the receptor. Henceforth referred to as α-bungarotoxin binding peptide (BTB), this oligopeptide is able to bind to the snake-venom α-bungarotoxin with high-affinity in the nanomolar range [32,33]. It has been demonstrated that receptors tagged with this BTB site can be visualized by addition of fluorescence-labeled α-bungarotoxin [3,34,38]. The α-bungarotoxin-BTB reporter system has several advantages. First, α-bungarotoxin has a molecular mass of only ~8 kDa, and thus it is considerably smaller than other reporter proteins, such as antibodies or any of the fluorescent proteins. Second, α-bungarotoxin is membrane impermeant and, when applied to living cells, allows a selective labeling of functional BTB-tagged receptors at the plasma membrane excluding signals from the cell interior. Moreover, receptor tracking and pulse-chase studies are possible.
We provide evidence that the usage of this reporter system in combination with an appropriate high-affinity antagonist allows to monitor conformational changes of the oxytocin receptor.

EXPERIMENTAL

Reagents

Reagents were provided from the following supplier: Alexa Fluor 568 and Alexa Fluor 647 carboxylic acid, succinimidyl ester, α-bungarotoxin-Alexa Fluor 647, α-bungarotoxin-tetramethylrhodamine, Lipofectamine 2000, Invitrogen; primers and sequencing oligonucleotides, Genterprise (Mainz); Mowiol, Calbiochem (Bad Soden); restriction enzymes, and Phusion DNA polymerase, Fermentas (St. Leon-Rot) and NEB (Frankfurt); petri dishes, Sarstedt (Nuernbrecht, Germany); penicillin, streptomycin, bovine serum albumine, Roth (Karlsruhe, Germany); fetal calf serum (Gold), L-glutamine, Dulbecco´s modified Eagle medium, Minimal essential medium, trypsine, and hygromycin B, PAA (Linz, Austria); plasmid purification kit NucleoSpin, Macherey & Nagel (Dueren, Germany); gel extraction and PCR purification kits, Quiagen (Hilden, Germany); F792 antagonist (designated as OTAN), Ferring Pharmaceutics (Malmö, Sweden); [*Tyrosyl*-2,6-^{3}H]oxytocin (NET-858, 48.5 Ci/mmol, 32 Ci/mmol), NEN Du Pont de Nemours (Bad Homburg). DChol was synthesized by our group [37]. All other substances except stated otherwise were purchased from Sigma-Aldrich (Deisenhofen, Germany).

Synthesis of OTAN-Alexa Fluor 568 (OTAN-A568) and OTAN-Alexa Fluor 647 (OTAN-A647)

Alexa Fluor 568 and Alexa Fluor 647 carboxylic acid, succinimidyl ester (A568 and A647, respectively) (each 1 mg; ~1.3 µmol) was first dissolved in 60 µl dimethylformamide (anhydrous). The oxytocin antagonist OTAN (Ferring compound 792, designated here as OTAN) (0.8 mg; 0.9 µmol) was dissolved in 80 µl

dimethylformamide (anhydrous) and was mixed with solution A568 and A647, respectively. Triethylamin (1 µl) and 300 µl methanol were added to this mixture. The pH value of the mixture was >8 as controlled. The reaction was allowed to proceed for about 20 h under light protection. The proceeding of the reaction was controlled by HPLC analysis of small aliquots at different time points. The reaction was stopped by addition of 4 ml of solution A (H_2O/0.1% TFA). An aliquot of this reaction mixture was injected on a HPLC reversed-phase column (Vydac C8: 5 µm). Elution was performed with the following gradient of solution A (H_2O, 0.1% TFA) and solution B (90% acetonitrile, 10% H_2O, 0.1% TFA) at a flow rate of 1 ml/min: from 10% B to 30% B for 10 min and from 30% B to 90% B for 40 min. Peak fractions containing the reaction product were collected and analyzed. The calculated molecular masses of both OTAN-A568 and OTAN-A647 were confirmed by mass spectroscopy (Ciphergen Biosystems, Camberley, U.K.).

Oxytocin receptor constructs

BTB tags were introduced at different positions of the OTR. The plasmid pfmOTRh encoding the human oxytocin receptor including small epitope tags for flag (f), myc (m) at the N-terminal and poly-His (h) at the C-terminal part of the receptor was used as a starting point for the cloning of the different constructs described below. The cloning of the similar plasmid pmOTRf has been described [10]. For the first construct, the plasmid pfmOTRh was cut with *Hind*III and *BamH*I. To generate the double strand BTB-adapter at the N-terminus of the oxytocin receptor, the following primers were annealed: 5'-AGCTTGGTACC**ATG**GGATGGAGATACTACGAGAGCTCCCTGGAGCCCTACC CTGACTTG-3´ (forward) and 5´-GATCCAAGTCAGGGTAGGGCTCCAGGGAGCTCTCGTAGTATCTCCATCCCAT GGTACCA-3´ (reverse). This adapter consists of a BTB site (peptide WRYYESSLEPYPD) (Fig. 1A) including a START codon (bold), a *Kpn*I site (underlined) necessary for the next cloning reaction (see below) and cohesive ends compatible to ligation with *BamH*I and *Hind*III. The primers were annealed in a thermocycler and were ligated to the vector pfmOTRh digested with *BamH*I and *Hind*III. The resulting expression plasmid is designated pOTR-BTBe1. In a second construct, the EGFP tag was introduced at the C-terminus of the oxytocin receptor construct OTR-BTBe1. For this purpose, pOTR-BTBe1 (~6.6 kb) was digested with *Kpn*I that cuts the plasmid at two sites. The first site is within the BTB adapter before the start codon, the second site is shorthly before the stop codon of the oxytocin receptor. The insert (~1.2 kb) encoding the OTR-BTB was purified. The vector pEGFP-N3 (Clontech) was cut with *Kpn*I, was dephosphorylated to prevent self-ligation and was ligated with the insert OTR-BTB. The plasmid that contained OTRGFP-BTB in the correct orientation was designated pOTRGFP-BTBe1. In the third construct, the BTB tag was inserted into the third extracellular loop (e4 see Fig. 1B). PCR reactions were employed to introduce two restriction sites (*EcoR*I and *EcoR*V) into the cDNA sequence encoding this loop. The PCR reactions were performed with Phusion Polymerase using the following primers: P1, 5´-AAGCGTGTACGGTGGGAGGTC-3´; P2, 5´-GGGATATCCGCCCCCGGAATTCCCGGCATCCCAGACGCTCCACATCTG-3´; P3, 5´-GGGAATTCCGGGGGCGGATATCCCAACGCGCCCAAGGAAGCCTCGGCC-3´; P4, 5´-CAGAATAGAATGACACCTACTC-3´. The primers P2 and P3 possess at their

5′ end cleavage sites for *EcoR*I and *EcoR*V and at their 3′-end nucleotides complementary to the cDNA encoding the oxytocin receptor. Additionally, P2 and P3 were complementary to each other at their 5′ ends. Using the plasmid pfmOTRh as template, the first two PCR reactions were performed with the primers P1 and P2 (PCR1) and P3 and P4 (PCR2), yielding products of ~1.2 kb and ~0.6 kb, respectively. The PCR products were purified and used in stoichiometric amounts together with the primers P1 and P4 for a third PCR reaction. In the first round of this reaction, the complementary products of PCR1 and PCR2 hybridize and undergo a fill-in reaction at their 3′ ends. Thereafter, the PCR starts and amplifies a ~1.7 kb product that encodes the oxytocin receptor with the inserted *EcoR*I and *EcoR*V sites. This linear 1.7 kb DNA sequence was purified, digested with *Nhe*I and *Kpn*I. The ~0.6 kb *Nhe*I-*Kpn*I fragment was isolated and cloned into the vector pfmOTRf cut by *Nhe*I and *Kpn*I. The resulting plasmid now contained the coding sequence for the oxytocin receptor including the *EcoR*I and *EcoR*V sites at positions appropriate for the insertion of the BTB adapter oligonucleotides. The plasmid was cleaved with *EcoR*I and *EcoR*V and the BTB adapter was inserted. The following primers were hybridized to obtain the BTB adapter with compatible ends for ligation with *EcoR*I and *EcoR*V: 5′-AATTCCTGGAGATACTACGAGAGCTCCCTCGAGCCCTACCCTGACG-3′ (forward) and 5′-CGTCAGGGTAGGGCTCGAGGGAGCTCTTCGTAGTATCTCCAGG-3′ (reverse). Following successfull ligation the resulting clone was designated pfmOTRBTBe4. The identities of the various constructs were confirmed by DNA sequencing.

Cell culture, transfection and expression

All cells were cultured in monolayers in complete Dulbecco's modified Eagle's medium (DMEM) supplemented with penicillin, streptomycin, and 10% (v/v) fetal calf serum. HEK293 fibroblasts were transfected with the different constructs using Lipofectamine 2000. To obtain stably expressing cells, the transfected cells were incubated for 24 h, split and selected with 1 mg/ml G418. Several neomycin-resistant cell clones were propagated and screened for [^{3}H]oxytocin binding activity.

Membrane preparation

Cells were centrifuged at 100 x g for 10 min. The cell pellet was washed twice with phosphate-buffered saline (PBS) and resuspended in homogenization buffer (5 ml per 100 ml of cells) containing 20 mM Hepes, pH 7.4, 5 mM EDTA, and a protease inhibitor cocktail composed of bacitracin, soybean trypsin inhibitor, leupeptin, and phenylmethylsulfonyl fluoride. The suspension was homogenized using a Polytron PT-10. This was followed by homogenization using a Dounce glass homogenizer (10 strokes). Subsequently the homogenate was centrifuged at 40,000 x g for 30 min and the pellet was washed once with homogenization buffer. For some experiments, these ´crude membranes` were further purified by sucrose density gradient centrifugation as described [13]. Briefly, the membranes (5-10 mg protein) was resuspended in homogenization buffer and was layered on top of a stepwise gradient consisting of 3.5 ml of 60% (w/v) sucrose and 4 ml of 35% (w/v) sucrose prepared in homogenization buffer. After centrifugation at 115,000 x g for 90 min (SW-41 rotor) the membranes at the upper 0-35% sucrose interface were collected and diluted with binding buffer containing 20 mM Hepes, pH 7.4, 5 mM $MgCl_2$, trypsin inhibitor, and bacitracin. The

membranes were centrifuged for 1 h at 165,000 x g (Ti60 rotor), were resuspended in binding buffer and were shock-frozen in liquid nitrogen and stored at -70°C.
The Bradford method was used to quantify the protein content of the samples, with bovine serum albumin as standard.

Receptor binding assays

To measure the ligand binding activity, membranes (100 µg) were incubated with [^{3}H]oxytocin (5-10 nM) in a total volume of 100 µL binding buffer for 30 min at 30°C. Association experiments were performed by incubating the membranes with 3 nM of [^{3}H]oxytocin at 30°C for various times until the equilibrium binding was achieved (30 min). Then, the dissociation of the ligand-receptor complex was initiated by addition of a 1000 fold excess of unlabeled oxytocin. The binding reaction was stopped by addition of ice-cold binding buffer (10 mM Tris, pH 7.4, 5 mM $MgCl_2$) and bound ligand was separated from free ligand by rapid filtration over Whatman GF/F filters presoaked with 0.3% poly(ethylenimine). Filters were incubated with 10 mL scintillation cocktail (Filter-Count, Perkin-Elmer) and were counted. Nonspecific binding was determined in the presence of a 700-1000-fold excess of unlabeled oxytocin.
In saturation experiments with fluorescent ligands (αBT-A568 or OTAN-A568), membranes (50 – 100 µg) were incubated for 30 min at 30°C with increasing ligand concentrations in binding buffer (100 µl). Unbound ligand was removed by centrifugation (5 min, 21,000 g, 4°C), followed by two washing steps with 1 ml each of ice-cold binding buffer. Finally, the membranes were resuspended in 1 ml methanol, in which the fluorescence was measured spectrofluorimetrically (Quantamaster, PTI) using excitation and emission wavelengths of 578 nm and 600 nm, respectively.
All assays were carried out in triplicate. Data analysis of the binding studies was performed using nonlinear curve fitting algorithms (GraphPad). Graphical output was performed by Sigmaplot version 8.0 (Systat Software Inc.).
Radioligand binding assays on whole cells stably transfected with oxytocin receptors were carried out as described. Data were analyzed using LIGAND and IC_{50} values were converted to pK_i values (- log of the inhibition constant K_i) using the Cheng-Prusoff equation: $K_i = IC_{50}/(1 + ([L]/K_D)$, where IC_{50} is the concentration of competing ligand which displaces 50% of the specific binding of the radioligand, [L] is the concentration of the radioligand, and K_D is the dissociation constant of the radioligand-receptor interaction.

Alteration of the cholesterol content in the membranes

Extraction of cholesterol from the plasma membranes was carried out as previously described [10]. Briefly, membranes (5 mg/mL) were incubated with MβCD (final concentration 30 mM) for various times at 30°C. Thereafter, the membranes were washed twice and were resuspended in assay buffer. According to this protocol 70-85% of the initial cholesterol (35 µg/mg protein) could be removed from the membranes. To enrich the plasma membranes with cholesterol, we employed cholesterol-MβCD inclusion complexes [10]. Cholesterol (final concentration 3 mM) was added to an aqueous solution of MβCD (40 mg/mL). The mixture was overlaid with nitrogen, and was continuously vortexed under light protection for 24 h at 30°C in a thermomixer. The solution was filtered prior to use. The cholesterol-depleted membranes were incubated with cholesterol-MβCD (final concentration 0.3 mM of cholesterol in complex) for various times to restore their cholesterol content.

Lipid extraction and determination of cholesterol

Lipids including cholesterol were extracted the method of Bligh and Dyer, slightly modified as described [12]. Briefly, 200 µL of membranes (10 µg - 1 mg protein) and 0.75 mL chloroform/methanol (1 : 2, v/v) were vigorously mixed for 10 min at 30°C in a thermomixer and centrifuged for 10 min at 21,000 g. The supernatant was mixed with 250 µL chloroform and 250 µL water and was centrifuged for 30 min at 21,000 g. The bottom lipid phase was evaporated under a N_2 atmosphere and was dissolved in isopropanol.

Cholesterol was assayed spectrophotometrically using a Diagnostic kit (R-Biopharm AG, Darmstadt, Germany) performed in a microscale dimension. Protein was determined by the Bradford assay (Roti-Quant and Roti-Nanoquant, Roth, Karlsruhe, Germany) using bovine serum albumin as standard.

Calcium measurements

For measurements of the cytosolic Ca^{2+} concentrations, cells grown on petri dishes to about 80% of confluency were loaded with fura-2 AM (1.5 µM) for 30 min at 37°C. Thereafter, the cells were scraped from the petri dishes and were resuspended in HBS buffer (20 mM Hepes, pH 7.4, 150 mM NaCl, 5 mM KCl, 1 mM $MgCl_2$, 1 mM $CaCl_2$, 1 mM glucose). Aliquots of the suspension (6 x 10^5 cells) were added to prewarmed HBS and transferred into a cuvette which was placed into a thermostated (37°C) holder. The cell suspension was continuously mixed by a magnetic stirrer. Oxytocin was applied to the cells and the changes of the $[Ca^{2+}]_i$ were monitored spectrofluorimetrically (Quantamaster, PTI). The emission wavelength was set at 510 nm and dual-wavelength excitations were performed at 340 nm and 380 nm, respectively (about 2 ratios/sec). The $[Ca^{2+}]_i$ was calculated by using the ratio 340/380 nm. The R_{max} value was obtained after Triton X-100 was added to the samples. Thereafter, minimum fluorescence (R_{min}) was obtained by chelating calcium with 5 mM EGTA and increasing the pH above 8.3. For the calculations of $[Ca^{2+}]_i$ a K_D of 225 nM between Ca^{2+} and fura-2 was assumed.

Fluorescence quenching experiments

Collisional quenching of free and bound probes, OTAN-A568 and αBT-A647, was analyzed fluorimetrically using the hydrophilic quenchers, potassium iodide (KI) and cobalt chloride ($CoCl_2$) as well as the lipid-soluble quencher TEMPO. Measurements were performed in assay buffer (20 mM Hepes, pH 7.4, 5 mM $MgCl_2$) with 50 nM of ligand. To monitor the quenching of membrane-bound probes, the ligands were added to 50 µg plasma membranes prepared from the indicated cells and were bound to equilibrium (30 min, 30°C). Excess ligand was washed off by centrifugation. Fluorescence was measured in a thermostated (20°C) cuvette after sequential additions of the quencher (from stock solutions of 1 M for $CoCl_2$ and KI) under continuous stirring. In case of KI, the stock was prepared in 10 mM NaS_2O_3 to prevent air-induced oxidation. The effects of dilution and ionic strength were calibrated by sequential additions of 1 M KCl to control samples. The quencher TEMPO was added from a 500 mM stock solution in ethanol. The hydrophobic quenching of TEMPO was verified using membranes in which the fluorescent cholesterol analog 6-dansyl-cholestanol (DChol) has been incorporated. For this purpose, 50 µg plasma membranes were incubated in a volume of 1 ml with 3 µl of 3 mM DChol-MßCD at 4°C for 20 min.

Thereafter, membranes were washed twice with assay buffer and were used for experiments. DChol-MßCD was prepared as described [37].
Excitation and emission wavelengths were set at the corresponding maxima, i.e. 578 nm and 600 nm for OTAN-A568, 647 nm and 670 nm for αBT-A647, and 360 nm and 510 nm for DChol. The data were background corrected and were plotted according to the Stern-Volmer equation, $F_0/F=1 + K_{SV}$ [Q], where F_0/F is the ratio of fluorescence intensity in the absence and presence of the quencher (Q). The Stern-Volmer constants K_{SV} were determined from the slope of F_0/F as a function of the quencher concentration.

Fluorescence anisotropy and FRET measurements
Plasma membranes from OTR expressing cells (50 µg) with normal or altered cholesterol content were incubated with OTAN-A568 or αBT-A647 (50 nM each) for 30 min at 30°C. After washing-off unbound ligands by centrifugation (for 20 min at 32,000 x g at 4°C) the membranes were resuspended in assay buffer, and the anisotropy of the corresponding fluorophore was measured. For that purpose, the membranes were transferred to a thermostated cuvette in a spectrofluorimeter (Quantamaster, PTI) and were continuously stirred at 20°C. Samples with OTAN-A568 or αBT-A647 were excited at 578 nm or 650 nm, respectively. The emission was measured at 600 nm for OTAN-A568 and 670 nm for αBT-A647. Slit widths of 5 nm were used at the excitation and emission site. The steady-state fluorescence, r, was determined according to $r = (I_{VV} - I_{VH}G)/(I_{VV} + I_{VH}G)$ where I_{VV} and I_{VH} are the fluorescence intensities observed with the excitation polarizer in the vertical position and the analyzing emission polarizer in both the vertical (I_{VV}) and the horizontal (I_{VH}) configurations. The factor G was used to correct for the unequal transmission of differently polarized light.
For most FRET measurements, the receptor-bound ligands OTAN-A568 and αBT-A647 were used as donor and acceptor fluorophores, respectively. For a series of control experiments, the receptor bound antagonists OTAN-A568 and OTAN-A647 were used as donor-acceptor pairs. The ligands were added either separately or together to plasma membranes prepared from OTR-BTBe1 and OTR-BTBe4 cells. After washing off unbound ligands by centrifugation (for 20 min at 32,000 x g at 4°C), the membranes were placed into a thermostated (20°C) cuvette under continuous stirring. The samples were excited at 578 nm and the emission fluorescence was scanned from 585-700 nm. Energy transfer, E, was calculated from the measured donor fluorescence intensity at 578 nm in the presence and absence of the acceptor according to $E = 1 - (F_{DA}/F_D)$ where F_D and F_{DA} are the donor intensities of samples containing only donor-labeled ligand (OTAN-A568) and samples with both donor- and acceptor-labeled ligands (OTAN-A568/αBT-A647 or OTAN-A568/OTAN-A647), respectively.

Fluorescence microscopy
For live cell microscopy, cells were grown in small petri dishes into which coverslips (diameter of 18 mm) were placed. Prior to addition of the cells, coverslips and dishes were coated with poly-D-Lysin. The coverslips were placed into a homemade chamber system where temperature and humidity are controlled. Unless stated otherwise, the cells were perfused with imaging buffer (10 mM HEPES, pH 7.4, 145 mM NaCl, 4.5 mM KCl, 1.2 mM $MgCl_2$, 1.2 mM $CaCl_2$, 10 mM glucose) containing the indicated concentrations of ligands/reagents. Microscopical images were aquired either on an epifluorescence system (Olympus Cell-R, Hamamatsu ORCA-ER) or on a confocal laser scanning microscope (Leica LSC-SP1, equipped with argon 488 nm, diode-

pumped solid-state 561 nm, and HeNe 633 nm laser) using the objectives 63x, 1.3 NA oil (Leica LSC-SP1) and 100x, 1.4 NA oil (Olympus system), respectively. Appropriate filter settings were used. If required, cells were fixed with 3.7% paraformaldehyde for 20 min at 23°C. Then, the cells were washed twice with phosphate buffered saline and were embedded with mowiol.

RESULTS

Expression and activity of the recombinant oxytocin receptors

We characterized the ligand binding behavior and the physiological responsiveness of the various oxytocin receptor constructs expressed in HEK293 fibroblasts. Three receptor constructs have been created. In the first construct, the BTB tag (Fig. 1A) has been incorporated at the amino terminus (e1) (see Fig. 1B). In the second one, EGFP has been fused at the C-terminus of the oxytocin receptor that additionally bears the BTB tag at the amino terminus. In the third construct, BTB was placed into the middle of the third extracellular loop e4 (Fig. 1B). The corresponding constructs were designated as OTR-BTBe1, OTRGFP-BTBe1, and OTR-BTBe4, respectively. Cells expressing EGFP at the C-terminus of the oxytocin receptor (OTRGFP-BTBe1) were created in order to compare the trafficking of the oxytocin receptor using the bungarotoxin-BTB *vs* the GFP reporter system. HEK293 fibroblasts expressing the same oxytocin receptor-EGFP fusion protein as found in the construct OTRGFP-BTBe1 but without BTB tag have recently been characterized [12]. The [^{3}H]oxytocin binding affinity of the later receptor construct was in the nanomolar range similar as found for the untagged oxytocin receptor [12]. The data of ligand binding parameters are summarized in Table 1. In saturation experiments with [^{3}H]oxytocin, high-affinity radioligand binding was observed for all oxytocin receptor constructs. Oxytocin receptors with both EGFP and BTB tag exhibit a slightly reduced affinity in [^{3}H]oxytocin binding. The expression level did not differ among the membranes from the three receptor constructs OTR-BTBe1, OTRGFP-BTBe1, and OTR-BTBe4. Moreover, all three oxytocin receptor constructs were functionally active. In response to oxytocin, they initiated transient increases of the intracellular calcium concentration. Supplementary Fig. S1 shows the percentage amplitudes of the corresponding calcium signals in dependence on the oxytocin concentration. The EC_{50} values of these responses correlate well with the corresponding K_D data of the three constructs (Table 1).

Characteristics of the fluorescent ligands used in this study

Next, we analyzed the properties of the fluorescent ligands used in this study. For this purpose, the following ligands were analyzed with respect to their potency as competitors of the [^{3}H]oxytocin binding to membranes from HEK293 cells expressing the oxytocin receptor: the agonist oxytocin, the partial agonist Arg-vasopressin (AVP), the antagonist OTAN, and the fluorescent antagonists OTAN-A568 and OTAN-A647. All ligands were able to displace the radioligand from the oxytocin receptor in a dose-dependent fashion (Fig. 2A). The IC_{50} values are given in the legend of Fig. 2. According to the equation of Cheng-Prusoff, the following corresponding K_i values were calculated: 4.5 nM for oxytocin, 36.8 nM for AVP, 2.0 nM for OTAN, 22.3 nM for OTAN-A568, and 21.5 nM for OTAN-A647. Thus, the fluorescent ligands OTAN-

A658 and OTAN-A647 were shown to displace [^{3}H]oxytocin binding with a roughly 10 fold less potency as compared to the unlabeled antagonist (structure see Fig. 2B) [39]. Thus, the attachment of the Alexa fluorophores maintained a reasonably high binding affinity to the oxytocin receptor. Further assays (e.g. the blocking of the oxytocin-induced calcium response) demonstrated that the antagonist remained its antagonistic behavior after its labeling with fluorophore (not shown).

The spectral properties of both OTAN-A568 and OTAN-A647 in different solvents were analyzed (Table 2). Only slight changes of the corresponding excitation and emission maxima were measured in polar *vs* nonpolar solvents. The relative emission intensities of OTAN-A568 varied from 53% to 162%, with the highest values detected in methanol. The environmental sensitivity of the fluorescence of OTAN-A647 was slightly lower than that of OTAN-A568. Overall, the fluorescence was relatively robust against changes of pH and high salt. Normalized excitation and emission spectra of both OTAN-A568 and OTAN-A647 dissolved in buffer are shown in Fig. 2C.

Binding of α-bungarotoxin-A568 (αBT-A568) to BTB-tagged oxytocin receptors

The binding behavior of αBT-A568 to the different BTB-containing oxytocin receptor constructs was explored. The kinetics of αBT-A568 binding to cells expressing the receptor OTR-BTBe1 is illustrated in Fig. 3A. For the other constructs OTR-BTBe4 and OTRGFP-BTBe1, the association and dissociation curves of αBT-A568 occurred with a similar kinetics (not shown). At 16°C, equilibrium of αBT-A568 binding was achieved at ~30 min (Fig. 3A, filled circles). Receptor-bound αBT-A568 remained stable for at least 90 min (Fig. 3A, open circles). Dissociation of cell-surface bound αBT-A568 was initiated when excess unlabeled α-bungarotoxin was administered to these cells. Within ~20 min about 70% of the αBT-A568 dissociated from the oxytocin receptor (Fig. 3A, open squares). Best fitting of the kinetic binding data was obtained by one-phase exponential equations (see legend Fig. 3).

Plasma membranes prepared from HEK293 cells expressing the BTB-tagged oxytocin receptors were used for saturation experiments with αBT-A568 (Fig. 3B). All binding data were best fitted by one-site models. Accordingly, the following B_{max} and K_D values were calculated: 0.46 pmol/mg and 10.9 nM for OTR-BTBe1, 0.35 pmol/mg and 8.0 nM for OTR-BTBe4, 0.55 pmol/mg and 9.9 nM for OTRGFP-BTBe1. Thus, all receptor constructs showed similar high affinity for the ligand αBT-A568 (K_D ~ 10 nM).

Finally, we analyzed whether receptor bound αBT-A568 becomes internalized in response to oxytocin. For this purpose, living HEK293 cells expressing OTR-BTBe1 were imaged at constant temperature (30°C) on a confocal microscope. After an incubation period of 30 min with αBT-A568 (2 µg/ml) and a short washing step, oxytocin (1 µM) was added. The amount of receptor-bound αBT-A568 at the cell surface decreased within minutes. To quantitate this process, receptor sequestration from the cell surface was recorded for several regions of interest (ROIs). The kinetics of agonist-induced receptor internalization is illustrated in Fig. 3C for three different ROIs from the indicated cells (Fig. 3C, inset). Each data point represents the αBT-A568 fluorescence of the indicated ROI in a time-lapse experiment. The data were fitted according to exponential equations and yield an average half-time of ~6.2 min for receptor sequestration.

Binding of fluorescent ligands to BTB-tagged oxytocin receptors

We have created two fluorescent ligands of high specificity for BTB-tagged oxytocin receptors: a fluorescent antagonist such as OTAN-A568 (or OTAN-A647) and a fluorescence-labeled α-bungarotoxin as αBT-A568. Their binding to HEK293 cells expressing the oxytocin receptor OTR-BTBe1 was further studied by imaging experiments. When OTAN-A568 or OTAN-A647 (each 100 nM) was applied to these cells, a distinct fluorescence labeling of the plasma membrane appeared (Fig. 4A, left panel for OTAN-A568, and Fig. 4D, right panel for OTAN-A647). In control experiments with untransfected HEK293 fibroblasts, the plasma membrane remain unstained (Fig. 4A, middle panel, compare with corresponding transmission image in right panel).

In Fig. 3C, we have already shown that receptor-bound αBT-A568 undergoes oxytocin-induced sequestration from the plasma membrane within minutes. In cells expressing OTR-BTBe1, stimulation by oxytocin leads to a substantial decrease of surface-bound αBT-A568 (Fig. 4B, left panel) and translocation of fluorescence from the plasma membrane into vesicles (Fig. 4B, middle and right panel). Does the receptor-bound ligand αBT-A568 dissociate from the receptor somewhere after the internalization process? To address this issue, we employed HEK293 cells expressing the oxytocin receptor with two different tags, the BTB-tag and a covalently attached EGFP protein at the receptors´ C-terminus, i.e. the construct OTRGFP-BTBe1. The itineraries of receptor-associated αBT-A568 and the EGFP fluorescence in response to oxytocin were compared. Up to a period of ~15 min of agonist-induced endocytosis, internalized receptors labeled with EGFP (Fig. 4C, left) and αBT-A568 (Fig. 4C, middle) revealed nearly perfect colocalization (Fig. 4C, merge). However, at prolonged incubation times (>30 min) with oxytocin, colocalization of EGFP labeled receptors and αBT-A568 containing structures decreases (Fig. 4D). The right panel of Fig. 4D shows the magnified inset of a region where separation of both fluorescence signals is particularly pronounced. Thus, fluorescent α-bungarotoxin remains associated with the receptor during the early phases of endocytosis. Later on (after 30-60 min of agonist stimulation) both molecules separate from each other and translocate into different populations of endosomes. The further fate of αBT-A568 (e.g. its possible degradation) has not been explored in this study.

Cholesterol dependence of ligand binding to BTB-tagged oxytocin receptors

Agonist binding of the oxytocin receptor strongly depends on the presence of cholesterol. We compared the binding of the ligands oxytocin (i.e. radiolabeled agonist [^{3}H]OT), OTAN-A568 (fluorescent antagonist), and αBT-A568 (fluorescent α-bungarotoxin) to the oxytocin receptor OTR-BTBe1 with respect to their cholesterol dependence. For that purpose, plasma membranes from HEK293 cells expressing OTR-BTBe1 were first incubated to equilibrium (30 min, 30°C) with [^{3}H]OT (100 nM), OTAN-A568 (1 µM), or αBT-A568 (2 µg/ml). Then, these membranes were (or were not) further subjected to cholesterol depletion by treatment with methyl-β-cyclodextrin (MβCD) (10 mM). This treatment decreased the cholesterol content from 201 ± 5 µg/mg protein to 62 ± 4 µg/mg protein (i.e. ~70% reduction). In cholesterol-depleted membranes, receptor binding of [^{3}H]OT and OTAN-A568 was dramatically decreased (Fig. 5A). When cholesterol was restored to normal (i.e. ~200 µg/mg protein) by incubating the cholesterol depleted membranes in the presence of the cholesterol donor

Chol-MβCD, binding of both [^{3}H]OT and OTAN-A568 was fully recovered. In contrast, the binding of αBT-A568 to the receptor remained unaffected irrespective of the membrane cholesterol content (Fig. 5A). Thus, in contrast to agonists and antagonists, α-bungarotoxin binds the BTB-tagged oxytocin receptor OTR-BTBe1 independent of the presence of cholesterol in the membrane. The same ligand-binding behavior was obtained when, instead of OTRBTBe1, the construct OTR-BTBe4 was used (not shown).

The observed cholesterol dependence of OTAN-A568 binding to the oxytocin receptor was analyzed in more detail. For this purpose, purified plasma membranes from HEK cells expressing OTR-BTBe4 were prepared and their cholesterol concentration was varied by using the cyclodextrin method. Successive depletion of cholesterol was achieved by increasing exposure times of the plasma membranes to the cholesterol acceptor MβCD (10 mM at 30°C) yielding a reduction of cholesterol from 201 ± 6 µg/mg protein (untreated = 100%) down to 59 ± 7 µg/mg protein. To obtain cholesterol-enriched membranes, plasma membranes were incubated for different times with the cholesterol donor Chol-MβCD (0.3 mM at 30°C). This increased their cholesterol content up to 300 ± 7 µg/mg protein (~50% above untreated membranes). The binding of OTAN-A568 to membranes with varying cholesterol contents is shown in Fig. 5B. A marked decrease in OTAN-A568 binding was observed when membrane cholesterol was reduced below ~130 µg/mg protein (i.e. ~35% decrease of cholesterol). We also performed saturation analysis with increasing OTAN-A568 concentrations to both cholesterol-depleted (~35% below normal) and cholesterol-enriched (~50% above normal) membranes from HEK293 cells expressing OTR-BTBe4, yielding the following K_D and B_{max} values: 18 ± 4 nM and 0.6 ± 0.1 pmol/mg protein for cholesterol-enriched, 27 ± 6 nM and 0.5 ± 0.1 pmol/mg protein for the cholesterol-depleted membranes (see Supplementary Fig. S2). When membranes were further cholesterol-depleted, the affinity to OTAN-A568 was drastically diminished (K_D > 100 nM) similar as previously described for the ligand oxytocin [12].

Probing the accessibility of bound ligands by collisional quenching in dependence on cholesterol

The water-soluble quenchers potassium iodide (KI) and cobalt chloride ($CoCl_2$) were used to probe the accessibility of free versus bound fluorescent labeled ligands OTAN-A568 and αBT-A647. For both quenchers, linear Stern-Volmer plots were obtained indicated collisional quenching. This is demonstrated in Supplementary Fig. S3 A for OTAN-A568 bound to plasma membranes prepared from OTR-BTBe4 cells. The Stern-Volmer constants K_{SV} represent the slopes of F_0/F as a function of the quencher concentration and provide information about the degree of accessibility of the fluorophore to the quencher. The K_{SV} values are displayed in Table 3. For both fluorescent ligands, quenching by the cationic cobalt was more pronounced than by the anionic iodide. Notably, the quenching constants of the free and receptor bound ligands OTAN-A568 and αBT-A647 were more or less the same. Surprisingly, nonspecifically bound OTAN-A568 appears to be slightly more exposed to the iodide quencher than the free or receptor bound antagonist.

Additionally, we performed experiments with the lipid-soluble quencher TEMPO. To verify whether TEMPO is able to quench molecules within the hydrophobic environment, the fluorescent cholesterol analog DChol recently synthesized by our group [37] was incorporated into the plasma membrane using DChol-loaded MßCD and

its quenching by TEMPO was measured. As shown in Supplementary Fig. 3S B (open circles), DChol was efficiently quenched by TEMPO (K_{SV} ~ 80 M^{-1}). In contrast, quenching of the fluorescence of receptor-bound OTAN-A568 by TEMPO was negligible (Fig. 3S B, filled circles).

Next, we asked whether changes of the cholesterol content in the plasma membrane from OTR-BTBe4 expressing cells affected the solvent accessibility of the receptor-bound antagonist. Lowering the cholesterol level beneath a certain threshold can dramatically decrease the binding of antagonist OTAN-A568 as shown in Fig. 5B. Thus, we decreased the membrane cholesterol only slightly remaining above the level that was necessary to support the high-affinity binding of the antagonist as shown above. This was achieved by a substantial shortened exposure time of the membranes to the MβCD (10 mM for 5 min at 30°C). Under this condition, ~20% of the initial cholesterol was extracted (=′- Chol`, i.e. cholesterol reduction from 201 ± 6 µg/mg protein to 155 ± 5 µg/mg protein) and >95% of OTAN-A568 remained bound as compared to untreated membranes (=′Con`). To obtain cholesterol-enriched membranes, plasma membranes were incubated with Chol-MβCD (0.3 mM for 5 min at 30°C) to increase their cholesterol content by ~20% (=′+ Chol`, i.e. cholesterol increase to 247 ± 8 µg/mg protein) above untreated membranes. OTAN-A568 was bound to cholesterol-depleted (′-Chol`), cholesterol-enriched (′+Chol`) and untreated (′Con`) membranes and quenching was performed with KI, $CoCl_2$, or TEMPO (Supplementary Fig. 3S C, white, grey and black bars). In all cases, the corresponding quenching constants (K_{SV}) did not differ significantly among membranes with different cholesterol contents. Similar K_{SV} values were obtained in quenching experiments with membranes from OTRBTBe1 cells (data not shown). Thus, the solvent accessibility of the bound antagonist is not affected by the cholesterol level of the membrane.

Rotational freedom of bound ligands in dependence on cholesterol

To assess the degree of rotational freedom of the receptor-bound ligands, fluorescence anisotropy measurements were performed. Plasma membranes from OTR-BTBe4 expressing cells with normal (′Con`), decreased (′-Chol`) or increased (′+Chol`) cholesterol amounts were prepared as described above. Fig. 6 shows the fluorescence anisotropy values determined for the receptor bound antagonist OTAN-A568 (open bars) and αBT-A647 (filled bars), respectively, in membranes with different cholesterol contents. The corresponding cholesterol concentrations are given in the legend of Fig. 6. The fluorescence anisotropy (r) of receptor-bound OTAN-A568 was significantly increased in cholesterol-enriched membranes (r = 0.246 ± 0.015) compared with control (r = 0.21 ± 0.010) or cholesterol-depleted membranes (r = 0.20 ± 0.017). All these values are markedly higher than those measured for unbound OTAN-A568 (r = 0.065 ± 0.011) or for OTAN-A568 nonspecifically bound to bovine serum albumin (r = 0.124 ± 0.013). In case of αBT-A647, the receptor-bound anisotropy values were only slightly higher than that measured for the free ligand (r = 0.166 ± 0.013). The higher anisotropy value for unbound αBT-A647 compared with free OTAN-A568 is expected in view of the fact that the rate of rotational diffusion is inversely correlated with the size of the molecule; αBT-A647 is several fold larger (~8 kDa) than OTAN-A568 (~1,6 kDa). In membranes with different cholesterol contents, the fluorescence anisotropy data of receptor-bound αBT-A647 were almost identical.

FRET between receptor-bound ligands in dependence on cholesterol

Cholesterol-induced conformational changes of the oxytocin receptor might lead to changes of the distance and/or orientation of two ligands simultaneously bound to one receptor molecule. To address this issue, we employed FRET measurements with different combinations of appropriate FRET pairs. As a prerequisite for FRET, the emission spectrum of the donor has to overlap with the excitation spectrum of the acceptor fluorophore. The dyes Alexa Fluor-568 and Alexa Fluor-647 attached to the ligands OTAN or αBT form such a FRET pair. Plasma membranes prepared from cells expressing untagged (OTR) and BTB-tagged oxytocin receptors (OTR-BTBe1 and OTR-BTBe4) were incubated with different combinations of fluorescent ligands, OTAN-A568/αBT-A647 or αBT-A568/αBT-A647. After washing-off unbound ligands, FRET signals were analyzed spectrofluorimetrically. The results are shown in Table 4. Negligible ligand binding and no FRET signals were observed with control membranes from cells expressing untagged oxytocin receptors. This confirms the specificity of both ligands and excludes any contribution of energy transfer due to nonspecific ligand binding. When the ligand combination OTAN-A568 and αBT-A647 was applied to membranes prepared from cells expressing the BTB-tagged oxytocin receptor constructs OTR-BTBe1 and OTR-BTBe4, FRET between these ligands was clearly observed. Significantly larger FRET values were obtained for the construct OTR-BTBe4 compared to OTR-BTBe1 (Table 4). A typical FRET curve is displayed in Fig. 7A (emission scans from 585-700 nm with excitation at the donor excitation maximum of 578 nm). Energy transfer occurs from the FRET-donor OTAN-A568 (D, donor-only curve) to the FRET-acceptor αBT-A647 (A, acceptor-only) yielding a decreased fluorescence intensity of the donor emission (peak at ~600 nm) concomitant with increased sensitized emission of the acceptor fluorescence (peak at ~670 nm) (DA, donor-acceptor curve).

Finally, we used OTR-BTBe4 to analyze the influence of cholesterol on FRET between receptor-bound OTAN-A568 and αBT-A647. For this purpose, the plasma membranes from OTR-BTBe4 expressing cells were adjusted to six different cholesterol concentrations within the range from 130-300 µg/mg protein by treatments with MβCD/Chol-MβCD. For better comparison, we selected the same cholesterol concentrations (within the range mentioned above) used to analyze the cholesterol dependence of ligand binding to BTB-tagged oxytocin receptors (see section above and Fig. 5B). FRET efficiency between OTAN-A568 and αBT-A647 clearly increased in parallel with the cholesterol content in the membranes from OTR-BTBe4 expressing cells as shown in Fig. 7B. The corresponding FRET efficiencies and membrane cholesterol levels were positively correlated with a correlation coefficient close to 1 ($r^2 = 0.9641$).

Oxytocin receptors that are localized in close proximity within the plasma membrane, e.g. forming dimers or clusters, could also contribute to and disturb intramolecular FRET signals. To prove this possibility, we co-incubated BTB-tagged oxytocin receptors with the ligand combination αBT-A568 and αBT-A647, as well as with the antagonist combination OTAN-A568 and OTAN-A647. However, no FRET signals were detectable in all of these samples (Table 4). This suggests that intermolecular receptor interactions, if present at all, occur rather infrequently, and should not contribute significantly to the observed FRET signals.

DISCUSSION

A direct interaction of the oxytocin receptor with cholesterol is supported by the following features: (i) agonist binding and receptor stability are highly dependent on cholesterol and exhibit a strong requirement on the specific structure of cholesterol [10,11]; (ii) the oxytocin receptor is markedly more stabilized in cholesterol-rich microdomains than in cholesterol-poor domains [12]; (iii) the receptor displays a specific dependence on cholesterol even in its solubilized form [11,12]; (iv) two putative cholesterol binding domains are found within the oxytocin receptor, termed as ´cholesterol consensus motif` [16] and ´cholesterol recognition amino acids consensus` sequence [9,23].

To explore putative conformational changes of the oxytocin receptor in dependence on cholesterol, we exploited the fluorescence properties of specifically bound ligands at varying cholesterol levels. For this purpose, we have created recombinant oxytocin receptors that are able to bind two small-sized ligands simultaneously. To achieve this goal, a short (13-amino acid) α-bungarotoxin binding site was inserted at the N-terminus (construct OTR-BTBe1) or within the third extracellular loop connecting transmembrane helices 6 and 7 (construct OTR-BTBe4). Cells expressing EGFP at the C-terminus of the oxytocin receptor (OTRGFP-BTBe1) were produced to compare the trafficking of the oxytocin receptor tagged with bungarotoxin-BTB *versus* EGFP. All receptor constructs were functionally active and bound both ligands, a specific receptor antagonist (OTAN) and α-bungarotoxin with high-affinity. The simultaneous receptor binding of both α-bungarotoxin and antagonist is supported by several observations: (i) Roughly equal amounts of binding sites have been calculated in saturation studies with both ligands. (ii) Even if a saturating concentration of one ligand (e.g. OTAN) has occupied the oxytocin receptors, similar amounts of the second ligand (e.g. labeled α-bungarotoxin) were still able to bind to the preoccupied receptors. Any displacement of the prebound first ligand by application of the second ligand has not been observed. (iii) Oxytocin that shares a partly common binding site with OTAN induces internalization of all α-bungarotoxin bound receptors, with a nearly perfect colocalization during the early phases (up to 30 min) of endocytosis. Thereafter, colocalization of ligand and receptor diminished gradually indicating different itineraries for both molecules. The majority of oxytocin receptors are known to recycle back to the plasma membrane, whereas the ligand becomes probably degraded in lysosomes [7].

Agonist and, to a slightly lesser extent, antagonist binding of the oxytocin receptor strongly depended on the presence of cholesterol, in agreement with our previous studies [10,11,15]. In contrast, fluorescent α-bungarotoxin (αBT-A568) bound to all BTB-tagged oxytocin receptor constructs independent of the cholesterol status in the membrane. This might be expected for construct OTR-BTBe1 in which α-bungarotoxin binds at the N-terminus presumably distant from the membrane bilayer. The fact that this is also observed for construct OTR-BTBe4 suggests that cholesterol-induced changes in the receptor conformation are not accompanied by significant changes in the position of the small extracellular loop 3.

The solvent accessibility of the fluorophores attached to both ligands was assessed by the influence of various types of quenchers. The accessibility of the water-soluble quenchers KI and $CoCl_2$ did not change upon association with the receptor. This was expected for αBT-A647 as the position of the fluorophore attached to α-bungarotoxin should not change dramatically. However, iodide quenching of both Alexa-labeled

ligands was relatively low. For example, in the cases of the secretin and cholecystokinin receptors, iodide quenching of Alexa Fluor 488 coupled ligands yielded several fold higher K_{SV} values [17,18]. The higher quenching by Co^{2+} compared to the anionic iodide might be explained by the electrostatic attraction of cationic Co^{2+} to the negatively charged Alexa fluorophore. Notably, the solvent accessibility of the bound antagonist was not affected by the cholesterol level of the membrane. Additionally we used TEMPO, a small nitroxide-carrying quencher that is able to examine the possible location of a fluorescent ligand in a hydrophobic microenvironment [25,30]. While TEMPO efficiently quenched a fluorescent cholesterol analogue, a substantial quenching of the fluorescent receptor bound ligands OTAN-A568 and αBT-A647 was not observed, irrespective of the cholesterol content of the membrane. Thus, none of the fluorophores attached to the ligands appears to be located in a hydrophobic pocket or very close to the membrane. Interestingly, an antagonist structurally very similar to OTAN binds in a central receptor pocket with close contacts to the first two transmembrane segments [14]. The results of the quenching experiments suggest that the fluorophore of OTAN-A568 located at the acyclic side chain of the peptide protrudes out of these transmembrane segments. Notably, the polarity around the fluorophores of the receptor-bound ligands was completely unaffected by cholesterol.

Our fluorescence anisotropy data showed that cholesterol had no influence on the rotational motion of αBT-A647, whereas an increased cholesterol content restricted the rotational motion of receptor bound OTAN-A568. Thus, cholesterol acting as a stabilizer of the oxytocin receptor [11] might decrease the rotational freedom of the antagonist placed within the binding pocket.

To specify putative cholesterol-induced receptor changes, FRET measurements were performed with different combinations of ligands containing appropriate FRET-pair fluorophores. Using the ligand combination OTAN-A568 and αBT-A647, FRET between these ligands was clearly observed for both OTR-BTBe1 and OTR-BTBe4 receptors. However, the construct OTR-BTBe4 revealed considerably larger FRET values compared to OTR-BTBe1. We provide two lines of evidence that the FRET signals measured here are caused by intramolecular FRET, i.e. describe changes of receptor conformation and are not due to intermolecular FRET (e.g. the presence of receptor dimers/oligomers). Firstly, no FRET signals were detectable for the constructs OTR-BTBe1 or OTR-BTBe4 when the FRET pair αBT-A568/αBT-A647 was used. Secondly, we have employed antagonist OTAN-A647 that could act as a potential FRET acceptor for OTAN-A568 in the case when receptor dimerization occurs. Again, we observed no energy transfer in experiments using the donor/acceptor pair OTAN-568/OTAN-A647 bound to the receptor OTR-BTBe4. Nevertheless, it is important to note that our results do not rule out that oxytocin receptor dimers are present in cells expressing either of these constructs. Actually, oxytocin receptor dimers/oligomers have been described in 293T cells, COS cells and mammary glands of lactating rats using sensitive detection methods such as bioluminescence resonance energy transfer or lanthanide-based time-resolved fluorescence [1,8,36]. Perhaps, the higher sensitivities of these latter methods are more appropriate for the detection of intermolecular interactions.

The observed cholesterol-induced increase in FRET between OTAN-A568 and αBT-A647 could be caused either by changes in the orientation or in the distance of the fluorophores. The fluorescence quenching data suggested no major changes in the molecular environment of the fluorophores in response to modulation of the cholesterol

content. This would support the conclusion that the cholesterol-induced increase in FRET is primarily caused by decreasing the distance between the fluorophores. This interpretation of the data is illustrated in Fig. 8. Accordingly, the antagonist binding site is closer to the BTB site in extracellular loop e4 than to the BTB site in loop e1. Additional cholesterol decreases the distance between antagonist binding site and position e4. Whether the distance between antagonist binding site and the e1 site is also diminished by cholesterol, could not be proved because the corresponding FRET value was very low and close to the detection limit, possibly due to a high structural flexibility of the N-terminus of the receptor. However, the Alexa 568 dye revealed a low sensitivity to environmental changes and the fluorescence anisotropy of OTAN-A568 was found to be affected by cholesterol. Thus, cholesterol-induced changes in the dynamics of OTAN-A568 and possibly in its orientation might contribute to the observed changes in the FRET signal. The dipole orientation factor (κ^2) can not be directly measured and is the major uncertainty in the calculation of the Förster radius (R_0). Provided that both FRET probes exhibit free isotropic motion, κ^2 is assumed to have a value of 2/3. Under this assumption, a R_0 value of 82 Å was calculated for the dye pair Alexa Fluor 568 and Alexa Fluor 647 (from ´Molecular Probes Handbook`). If all the change in the FRET signal would come from the change in the distance between the fluorescently labeled ligands, one can calculate a ~10 Å decrease in distance between OTAN-A568 and αBT-A647 in response to cholesterol levels ranging from ~130 µg/mg protein (i.e. ~35% below normal) to ~270 µg/mg protein (i.e. ~30% above normal). Alternatively, cholesterol-induced alterations in the orientation of OTAN-A568 could lead to changes in κ^2 and, thus an altered R_0 value. Most likely, cholesterol causes a combination of both changes in orientation and distance of the receptor bound ligands.

Cholesterol is known to stabilize some GPCRs such as rhodopsin [2,20], the β_2-adrenergic receptor [16,40], the A_{2a} adenosin receptor [19], and the oxytocin receptor [11]. As cholesterol combines small size, flexibility (aliphatic side chain) and rigidity (tetracyclic ring system) in one molecule, it is ideally suitable to fill shallow grooves and cavities at the receptor surface, e.g. by occupying so-called nonannular lipid binding sites [26]. Cholesterol binding may increase the intramolecular occluded surface area of the receptor, leading to enhanced protein stability [16]. Molecular dynamics simulations also provided evidence that surface-bound or embedded cholesterol is essential for the stabilization and functioning of diverse membrane proteins [4,20]. Overall, cholesterol binding appears to be mostly associated with reduced conformational flexibility and tighter packing of the protein structure. In case of the oxytocin receptor, our results fully agree with the conclusion that cholesterol supports a more compact structure. The approach described in this study might also be applicable to other membrane proteins aimed to analyze corresponding conformational changes of the protein in their native membrane environment.

Table 1. Ligand binding and activity of oxytocin receptor constructs
Binding data were obtained from membranes prepared from HEK293 cells that have been stably transfected with the indicated constructs. All experiments were performed in triplicate and data shown are means ± S.E.

Receptor construct	K_D (nM)	B_{max} (pmol/mg)	EC_{50} (nM)[b]
OTR-BTBe1[a]	2.1 ± 0.2	0.4 ± 0.1	1.1 ± 0.3
OTR-BTBe4[a]	3.7 ± 0.8	0.5 ± 0.1	2.5 ± 0.5
OTRGFP-BTBe1[a]	8.2 ± 1.8	0.4 ± 0.1	6.2 ± 1.1

[a]The binding parameters K_D and B_{max} were calculated from saturation of [^{3}H]oxytocin to crude membranes from stably transfected cells.
[b]EC_{50} values were obtained from oxytocin-induced calcium responses in fura-2 loaded cells. Data are from [12] and Supplemetary Fig. S1.

Table 2. Spectral properties of the fluorescent antagonist OTAN-A568 and OTAN-A647
Measurements were performed with each of 100 nM of OTAN-A568 or OTAN-A647. The data are means ± standard deviation (n=3).

Solvent	OTAN-A568			OTAN-A647		
	excitation peak (nm)	emission peak (nm)	relative fluorescence (%)	excitation peak (nm)	emission peak (nm)	relative fluorescence (%)
Water	578	600	100 ± 5	650	661	100 ± 6
Methanol	579	599	162 ± 6	650	664	99 ± 7
Isopropanol	583	600	144 ± 5	654	666	68 ± 6
Ethanol	579	598	148 ± 8	653	666	87 ± 7
Acetonitrile	581	604	123 ± 6	653	665	61 ± 6
Buffer (pH 7.0)[a]	578	601	98 ± 5	649	661	96 ± 5
Buffer (pH 2.0)[a]	582	604	53 ± 5	650	660	69 ± 4
Buffer (pH 10.0)[a]	579	599	77 ± 7	650	661	96 ± 3
1 M NaCl[b]	579	601	64 ± 8	650	661	66 ± 5
1 M $CaCl_2$[b]	579	601	65 ± 6	651	660	52 ± 4

[a]The buffers were as follows: 20 mM HEPES for pH 7.0, 20 mM glycine for pH 2.0, and 20 mM sodium carbonate for pH 10.0
[b]The salts were dissolved in water

Table 3. Fluorescence quenching constants for the ligands OTAN-A568, OTAN-A647, and αBT-A647

Plasma membranes were prepared from cells expressing the OTR-BTBe1 receptor and were incubated with increasing concentrations of the indicated quencher. The Stern-Volmer constants (K_{SV}) were determined as described in the legend of Supplementary Fig. S3. Values represent the means ± S.E. of at least 4 experiments (n.d., not determined).

Ligand	Quencher	K_{SV} free	K_{SV} nonspecific bound	K_{SV} specific bound
		M^{-1}	M^{-1}	M^{-1}
OTAN-A568	KI	0.9 ± 0.5	3.8 ± 1.0	1.42 ± 0.6
OTAN-A568	$CoCl_2$	9.5 ± 1.2	8.8 ± 1.1	11.9 ± 1.4
OTAN-A568	TEMPO	n.d.	1.10 ± 0.2	1.13 ± 0.3
αBT-A647	KI	0.11 ± 0.05	n.d.	0.18 ± 0.09
αBT-A647	$CoCl_2$	4.8 ± 0.8	n.d.	4.5 ± 0.7
αBT-A647	TEMPO	n.d.	n.d.	1.07 ± 0.4

Table 4. FRET between fluorescent ligands bound to the oxytocin receptor
Plasma membranes were prepared from cells expressing untagged (OTR, negative control) and BTB-tagged oxytocin receptors (OTR-BTBe1 and OTR-BTBe4). The indicated combination of ligands was added to the membranes and FRET measurements were performed spectrofluorimetrically as described in the ´Experimental` section. The data are means ± standard deviation (n=4).

Oxytocin receptor construct	Donor (D)	Acceptor (A)	FRET ($1-F_{DA}/F_D$)
OTR	αBT-A568	αBT-A647	none
OTR	OTAN-A568	OTAN-A647	none
OTR-BTBe1	OTAN-A568	OTAN-A647	none
OTR-BTBe1	αBT-A568	αBT-A647	none
OTR-BTBe1	OTAN-A568	αBT-A647	0.055 ± 0.024
OTR-BTBe4	OTAN-A568	OTAN-A647	none
OTR-BTBe4	αBT-A568	αBT-A647	none
OTR-BTBe4	OTAN-A568	αBT-A647	0.130 ± 0.018

Figure Legends

Figure 1. Oxytocin receptor constructs used in this study

(**A**) The BTB peptide (dotted circle) comprises only 13 amino acids (sequence as indicated), forms a hairpin like structure, and binds with high-affinity to α-bungarotoxin (structure from NCBI, MMDB ID:17181, PDB ID: 1HAJ) [33]. (**B**), The human oxytocin receptor and its putative binding domains for oxytocin, peptide antagonists (dotted squares), G proteins (dashed squares). Black circles, residues conservative for the whole GPCR family; grey circles, residues conservative within the oxytocin/vasopressin receptor family; residues marked with 'Y', putative N-glycosylation sites; e1-e4, extracellular domains; i1-i3, intracellular loops; dashed line, transmembrane helices 1 and 2 and upper parts of transmembrane helix 7 are previously defined binding sites for oxytocin receptor antagonists.

Figure 2. Oxytocin receptor binding of the fluorescent antagonists OTAN-A568 and OTAN-A647 in comparison with related unlabeled receptor ligands

(A) Displacement of [^{3}H]oxytocin binding to membranes from HEK-OTR cells by Arg-vasopressin (AVP) (filled circles), OTAN-A568 (filled triangles), OTAN-A647 (filled squares), oxytocin (OT) (open circles), and OTAN (open squares). Radioligand displacement was assessed by incubating membranes from HEK-OTR cells (100 µg), and 10 nM [^{3}H]oxytocin with the various peptides at the indicated concentrations. Values of specific binding of [^{3}H]oxytocin were expressed as percent of the maximum radioligand binding which was obtained in the absence of a competitor. Data of a representative experiment are shown. Curve fitting was performed using the logistic function $y=100/(1+(x/IC_{50})^b)$. The fitted parameters were as follows: for oxytocin, IC_{50}=31 nM, b=1.62; for AVP, IC_{50}=254 nM, b=1.37; for OTAN, IC_{50}=14 nM, slope b=1.57; for OTAN-A568, IC_{50}=154 nM, b= 1.79; for OTAN-A647, IC_{50}=150 nM, b= 1.38. (**B**), Structure of OTAN conjugated to the fluorophore group R (=A568 or A647). **(C)**, Normalized excitation and emission fluorescence spectra of OTAN-A568 (solid line) and OTAN-A647 (dashed line) (each 50 nM) in 20 mM Hepes, pH 7.4.

Figure 3. Binding behavior of α-bungarotoxin-A568 (αBT-A568) to BTB-tagged oxytocin receptors

(A) Kinetics of αBT-A568 binding to HEK293 cells transfected with the oxytocin receptor construct OTR-BTBe1. To determine association data, cells (~10^5) were incubated for 0-40 min with 2 µg/ml αBT-A568 in Hepes-buffered culture medium at 16°C. Excess ligand was washed off by centrifugation and cell-bound fluorescence was measured by spectrofluorimetry (filled circles). After equilibrium binding has been achieved, the cells were further incubated in the absence of fluorescent α-bungarotoxin (open circles). Dissociation of cell-surface bound αBT-A568 was negligible for at least 90 min. Rapid dissociation of αBT-A568 was initiated by administration of excess

unlabeled α-bungarotoxin (open squares). The association data were fitted according to the equation $y=a\bullet(1-e^{-bx})$. For OTR-BTBe1 cells, the calculated parameters for the association data (filled circles) were a=102, b=0.184. Fitting of the dissociation data was performed according to the equation $y=y0+a\bullet e^{-bx}$ and yielded the parameters y0=22.7, a=2654.8, b=0.0886. **(B)** Saturation binding of membranes from HEK293 cells expressing OTR-BTBe1, OTR-BTBe4, or OTRGFPe1 receptors. The membranes (100 µg) were incubated to equilibrium (40 min, 22°C) with increasing concentrations of αBT-A568. The data were fitted according to the equation $y=Bmax\bullet x/(K_D+x)$. **(C)** Oxytocin-induced internalization of α-bungarotoxin-A568 bound to the cell surface of HEK293 cells expressing OTR-BTBe1 receptors. Cells cultivated on a coverslip in small petri dishes were transferred to an imaging chamber on a confocal microscope (constant temperature 30°C) and were incubated for 30 min with αBT-A568 (2 µg/ml). After a short washing step, oxytocin (1 µM) was added. In time-lapse experiments, the sequestration of receptor-bound αBT-A568 from the cell surface was recorded for the indicated regions of interest (ROI), and was analyzed by Leica Confocal software. The kinetic data were plotted and fitted according to the equation $y=a+b\bullet e^{-kx}$, with $\tau=\ln 2/k$. The average value of τ calculated for three typical ROIs was 6.2 min. Inset, cells with the indicated ROIs (bar, 10 µm).

Figure 4. **Binding of fluorescent ligands to HEK293 cells expressing BTB-tagged oxytocin receptors**

(A) The antagonist OTAN-A568 (100 nM) was applied to HEK293 fibroblasts expressing OTR-BTBe1 (left panel). OTAN-A568 did not label untransfected HEK293 cells (middle panel). The right panel shows a transmission image of the cells present in the middle panel. **(B)** Alexa 568 labeled α-bungarotoxin (αBT-A568) was added for 10 min at 30°C to HEK293 cells expressing OTR-BTBe1. Then, the cells were stimulated or not (left panel) with 1 µM oxytocin (OT) for 3 min (middle panel) or for 20 min (right panel) at 30°C. **(C)** To induce receptor internalization, cells expressing OTRGFP-BTBe1 were treated with oxytocin for 15 min at 30°C. During this early time of agonist-induced endocytosis, internalized receptors labeled with EGFP (green, left panel) and αBT-A568 (red, middle panel) colocalize (merge, right panel). **(D)** After prolonged incubation with oxytocin (60 min), colocalization of EGFP labeled receptors (green) and αBT-A568 (red) containing structures decreases. Middle panel, magnified inset of the marked region of the left panel. Right panel, labeling of HEK293 cells expressing OTR-BTBe1 with antagonist OTAN-A647 (bar in magnified inset, 2 µm; other bars, 10 µm).

Figure 5. **Cholesterol dependence of ligand binding to BTB-tagged oxytocin receptors**

(A) Membranes (100 µg) from HEK293 cells expressing OTR-BTBe1 were incubated with the indicated ligands [^{3}H]OT (100 nM), OTAN-A568 (1 µM), αBT-A568 (2 µg/ml) for 30 min at 30°C. Then, the membranes were treated in the absence or presence of the cholesterol acceptor MβCD (final 10 mM) for 30 min at 30°C. To

restore the cholesterol content of cholesterol depleted membranes, MβCD treated membranes were incubated with Chol-MβCD (0.3 mM) for 20 min at 30°C. Excess ligands and MβCD/Chol-MβCD were washed off by centrifugation and the receptor-bound ligands (radioactivity or fluorescence) were counted. The cyclodextrin treatments changed the cholesterol content from 201 ± 5 µg/mg protein (untreated) to 62 ± 4 µg/mg protein (i.e. ~70% reduction), and back to normal (200 ± 10 µg/mg protein). **(B)** Membranes (50 µg) from HEK293 cells expressing OTR-BTBe4 were incubated with OTAN-A568 (1 µM) for 30 min at 30°C. Successive depletion of cholesterol was achieved by increasing exposure times of the membranes to the cholesterol acceptor MβCD (10 mM at 30°C) yielding the indicated cholesterol contents. For cholesterol enrichment, membranes were incubated for different times with Chol-MβCD (0.3 mM at 30°C) to increase their cholesterol content to the indicated values. Excess ligands and MβCD/Chol-MβCD were washed off and the receptor-bound ligand was measured. All data are means ± standard deviation (n=3).

Figure 6. Anisotropy of fluorescent ligands bound to the BTB-tagged oxytocin receptor in dependence on cholesterol

Plasma membranes from OTR-BTBe4 expressing cells were either left untreated (´Con`), were depleted of cholesterol by MβCD (´-Chol`) or were cholesterol-enriched using Chol-MβCD (´+Chol`) as described in legend of Supplementary Fig. S3. The cholesterol concentrations for plasma membranes ´Con`, ´-Chol`, and ´+Chol` were 201 ± 6 µg/mg protein, 155 ± 5 µg/mg protein, and 247 ± 8 µg/mg protein, respectively. The membranes (50 µg) were incubated with OTAN-A568 (50 nM) (open bars) or αBT-A647 (50 nM) (filled bars) (50 µg) for 30 min at 30°C. Excess ligand was washed off by centrifugation and the fluorescence anisotropy was measured. The data are means ± standard deviation (n=3). *, significant difference compared to control (t-test, $p<0.005$).

Figure 7. FRET between the ligands OTAN-A568 and αBT-A647 bound to the oxytocin receptor OTR-BTBe4 in dependence on cholesterol

(A) Plasma membranes prepared from OTR-BTBe4 expressing cells were incubated with OTAN-A568 (donor, D) and αBT-A647 (acceptor, A) either separately or together. After washing-off any unbound ligands by centrifugation, the membranes were resuspended in assay buffer, and were transferred to a thermostated (20°C) cuvette under continuous stirring. The samples were excited at 578 nm and the emission fluorescence was scanned from 585-700 nm. The three curves are emission scans of donor-only (D), acceptor-only (A), and donor-acceptor (DA) membranes. The background-subtracted and normalized fluorescence intensities are shown. Emission maxima of donor and acceptor probe are indicated. **(B)** Plasma membranes from OTR-BTBe4 expressing cells were treated or not with MβCD/Chol-MβCD to change their cholesterol content as indicated using the same experimental conditions described in Fig. 5B. OTAN-A568 and αBT-A647 were both added to the membranes as donor and acceptor ligand, respectively. After washing off excess ligands and MβCD/Chol-MβCD, FRET measurements were performed spectrofluorimetrically as described in the

´Experimental` section. The percentages indicate the cholesterol changes compared with untreated membranes. All data are means ± standard deviation (n=3).

Figure 8. Model of the oxytocin receptor with the binding sites for antagonist (A) and α-bungarotoxin (e1 and e4)

The model (top view of the oxytocin receptor from the extracellular side) was constructed by homology modelling using ´EasyPred3D´ with rhodopsin as template [21]. The UCSF Chimera programme (www.cgl.ucsf.edu/chimera) was employed for graphical display. TM, transmembrane domains; E, extracellular loops; e1 and e4, positions at E1 and E4 where BTB sites have been included.

Acknowledgments

We thank Dr. Per Melin (Ferring Pharmaceutics, Sweden) for providing the antagonist F792, designated here as OTAN. We thank Christa Wolpert for excellent technical assistance.

References

1 Albizu, L., Cottet, M., Kralikova, M., Stoev, S., Seyer, R., Brabet, I., Roux, T., Bazin, H., Bourrier, E., Lamarque, L., Breton, C., Rives, M. L., Newman, A., Javitch, J., Trinquet, E., Manning, M., Pin, J. P., Mouillac, B. and Durroux, T. (2010) Time-resolved FRET between GPCR ligands reveals oligomers in native tissues. Nat. Chem. Biol. **6,** 587-594

2 Bennett, M. P. and Mitchell, D. C. (2008) Regulation of membrane proteins by dietary lipids: effects of cholesterol and docosahexaenoic acid acyl chain-containing phospholipids on rhodopsin stability and function. Biophys. J. **95,** 1206-1216

3 Bogdanov, Y., Michels, G., Armstrong-Gold, C., Haydon, P. G., Lindstrom, J., Pangalos, M. and Moss, S. J. (2006) Synaptic GABAA receptors are directly recruited from their extrasynaptic counterparts. EMBO J. **25,** 4381-4389

4 Brannigan, G., Henin, J., Law, R., Eckenhoff, R. and Klein, M. L. (2008) Embedded cholesterol in the nicotinic acetylcholine receptor. Proc. Natl. Acad. Sci. U. S. A **105,** 14418-14423

5 Burger, K., Gimpl, G. and Fahrenholz, F. (2000) Regulation of receptor function by cholesterol. Cell Mol. Life Sci. **57,** 1577-1592

6 Cherezov, V., Rosenbaum, D. M., Hanson, M. A., Rasmussen, S. G., Thian, F. S., Kobilka, T. S., Choi, H. J., Kuhn, P., Weis, W. I., Kobilka, B. K. and Stevens, R. C. (2007) High-resolution crystal structure of an engineered human beta2-adrenergic G protein-coupled receptor. Science **318,** 1258-1265

7 Conti, F., Sertic, S., Reversi, A. and Chini, B. (2009) Intracellular trafficking of the human oxytocin receptor: evidence of receptor recycling via a Rab4/Rab5 "short cycle". Am. J. Physiol Endocrinol. Metab **296,** E532-E542

8 Devost, D. and Zingg, H. H. (2003) Identification of dimeric and oligomeric complexes of the human oxytocin receptor by co-immunoprecipitation and bioluminescence resonance energy transfer. J. Mol. Endocrinol. **31,** 461-471

9 Gimpl, G. (2010) Cholesterol-protein interaction: methods and cholesterol reporter molecules. Subcell. Biochem. **51,** 1-45

10 Gimpl, G., Burger, K. and Fahrenholz, F. (1997) Cholesterol as modulator of receptor function. Biochemistry **36,** 10959-10974

11 Gimpl, G. and Fahrenholz, F. (2002) Cholesterol as stabilizer of the oxytocin receptor. Biochim. Biophys. Acta **1564,** 384-392

12 Gimpl, G. and Fahrenholz, F. (2000) Human oxytocin receptors in cholesterol-rich vs. cholesterol-poor microdomains of the plasma membrane. Eur. J. Biochem. **267,** 2483-2497

13 Gimpl, G., Klein, U., Reilander, H. and Fahrenholz, F. (1995) Expression of the human oxytocin receptor in baculovirus-infected insect cells: high-affinity binding is induced by a cholesterol- cyclodextrin complex. Biochemistry **34,** 13794-13801

14 Gimpl, G., Postina, R., Fahrenholz, F. and Reinheimer, T. (2005) Binding domains of the oxytocin receptor for the selective oxytocin receptor antagonist barusiban in comparison to the agonists oxytocin and carbetocin. Eur. J. Pharmacol. **510**, 9-16

15 Gimpl, G., Reitz, J., Brauer, S. and Trossen, C. (2008) Oxytocin receptors: ligand binding, signalling and cholesterol dependence. Prog. Brain Res. **170,** 193-204

16 Hanson, M. A., Cherezov, V., Griffith, M. T., Roth, C. B., Jaakola, V. P., Chien, E. Y., Velasquez, J., Kuhn, P. and Stevens, R. C. (2008) A specific cholesterol binding site is established by the 2.8 A structure of the human beta2-adrenergic receptor. Structure **16,** 897-905

17 Harikumar, K. G., Clain, J., Pinon, D. I., Dong, M. and Miller, L. J. (2005) Distinct molecular mechanisms for agonist peptide binding to types A and B cholecystokinin receptors demonstrated using fluorescence spectroscopy. J. Biol. Chem. **280,** 1044-1050

18 Harikumar, K. G., Hosohata, K., Pinon, D. I. and Miller, L. J. (2006) Use of probes with fluorescence indicator distributed throughout the pharmacophore to examine the peptide agonist-binding environment of the family B G protein-coupled secretin receptor. J. Biol. Chem. **281,** 2543-2550

19 Jaakola, V. P., Griffith, M. T., Hanson, M. A., Cherezov, V., Chien, E. Y., Lane, J. R., Ijzerman, A. P. and Stevens, R. C. (2008) The 2.6 angstrom crystal structure of a human A2A adenosine receptor bound to an antagonist. Science **322,** 1211-1217

20 Khelashvili, G., Grossfield, A., Feller, S. E., Pitman, M. C. and Weinstein, H. (2009) Structural and dynamic effects of cholesterol at preferred sites of interaction with rhodopsin identified from microsecond length molecular dynamics simulations. Proteins 76, 403-417

21 Lambert, C., Leonard, N., De, B., X and Depiereux, E. (2002) ESyPred3D: Prediction of proteins 3D structures. Bioinformatics. **18,** 1250-1256

22 Levitan, I., Fang, Y., Rosenhouse-Dantsker, A. and Romanenko, V. (2010) Cholesterol and ion channels. Subcell. Biochem. **51,** 509-549

23 Li, H., Yao, Z., Degenhardt, B., Teper, G. and Papadopoulos, V. (2001) Cholesterol binding at the cholesterol recognition/ interaction amino acid consensus (CRAC) of the peripheral-type benzodiazepine receptor and inhibition of steroidogenesis by an HIV TAT-CRAC peptide. Proc. Natl. Acad. Sci. U. S. A **98,** 1267-1272

24 Lingwood, D. and Simons, K. (2010) Lipid rafts as a membrane-organizing principle. Science **327,** 46-50

25 Megha, Bakht, O. and London, E. (2006) Cholesterol precursors stabilize ordinary and ceramide-rich ordered lipid domains (lipid rafts) to different degrees. Implications for the Bloch hypothesis and sterol biosynthesis disorders. J. Biol. Chem. **281,** 21903-21913

26 Paila, Y. D., Tiwari, S. and Chattopadhyay, A. (2009) Are specific nonannular cholesterol binding sites present in G-protein coupled receptors? Biochim. Biophys. Acta **1788,** 295-302

27 Pang, L., Graziano, M. and Wang, S. (1999) Membrane cholesterol modulates galanin-GalR2 interaction. Biochemistry **38,** 12003-12011

28 Pucadyil, T. J. and Chattopadhyay, A. (2004) Cholesterol modulates ligand binding and G-protein coupling to serotonin(1A) receptors from bovine hippocampus. Biochim. Biophys. Acta **1663,** 188-200

29 Pucadyil, T. J. and Chattopadhyay, A. (2006) Role of cholesterol in the function and organization of G-protein coupled receptors. Prog. Lipid Res. **45,** 295-333

30 Rasmussen, S. G., Carroll, F. I., Maresch, M. J., Jensen, A. D., Tate, C. G. and Gether, U. (2001) Biophysical characterization of the cocaine binding pocket in the serotonin transporter using a fluorescent cocaine analogue as a molecular reporter. J. Biol. Chem. **276,** 4717-4723

31 Rosenbaum, D. M., Rasmussen, S. G. and Kobilka, B. K. (2009) The structure and function of G-protein-coupled receptors. Nature **459,** 356-363

32 Sanders, T. and Hawrot, E. (2004) A novel pharmatope tag inserted into the beta4 subunit confers allosteric modulation to neuronal nicotinic receptors. J. Biol. Chem. **279,** 51460-51465

33 Scherf, T., Kasher, R., Balass, M., Fridkin, M., Fuchs, S. and Katchalski-Katzir, E. (2001) A beta -hairpin structure in a 13-mer peptide that binds alpha -bungarotoxin with high affinity and neutralizes its toxicity. Proc. Natl. Acad. Sci. U. S. A **98,** 6629-6634

34 Sekine-Aizawa, Y. and Huganir, R. L. (2004) Imaging of receptor trafficking by using alpha-bungarotoxin-binding-site-tagged receptors. Proc. Natl. Acad. Sci. U. S. A **101,** 17114-17119

35 Simons, K. and Toomre, D. (2000) Lipid rafts and signal transduction. Nat. Rev. Mol. Cell Biol. **1,** 31-39

36 Terrillon, S., Durroux, T., Mouillac, B., Breit, A., Ayoub, M. A., Taulan, M., Jockers, R., Barberis, C. and Bouvier, M. (2003) Oxytocin and Vasopressin V1a and V2 Receptors Form Constitutive Homo- and Heterodimers during Biosynthesis. Mol. Endocrinol. **17,** 677-691

37 Wiegand, V., Chang, T. Y., Strauss, J. F., III, Fahrenholz, F. and Gimpl, G. (2003) Transport of plasma membrane-derived cholesterol and the function of Niemann-Pick C1 Protein. FASEB J. **17,** 782-784

38 Wilkins, M. E., Li, X. and Smart, T. G. (2008) Tracking cell surface GABAB receptors using an alpha-bungarotoxin tag. J. Biol. Chem. **283,** 34745-34752

39 Wisniewski, K., Trojnar, J., Riviere, P., Haigh, R., Yea, C., Ashworth, D., Melin, P. and Nilsson, A. (1999) The synthesis of a new class of oxytocin antagonists. Bioorg. Med. Chem. Lett. **9,** 2801-2804

40 Yao, Z. and Kobilka, B. (2005) Using synthetic lipids to stabilize purified beta2 adrenoceptor in detergent micelles. Anal. Biochem. **343,** 344-346

Biochemical Journal Immediate Publication. Published on 12 May 2011 as manuscript BJ20101795

Fig. 1

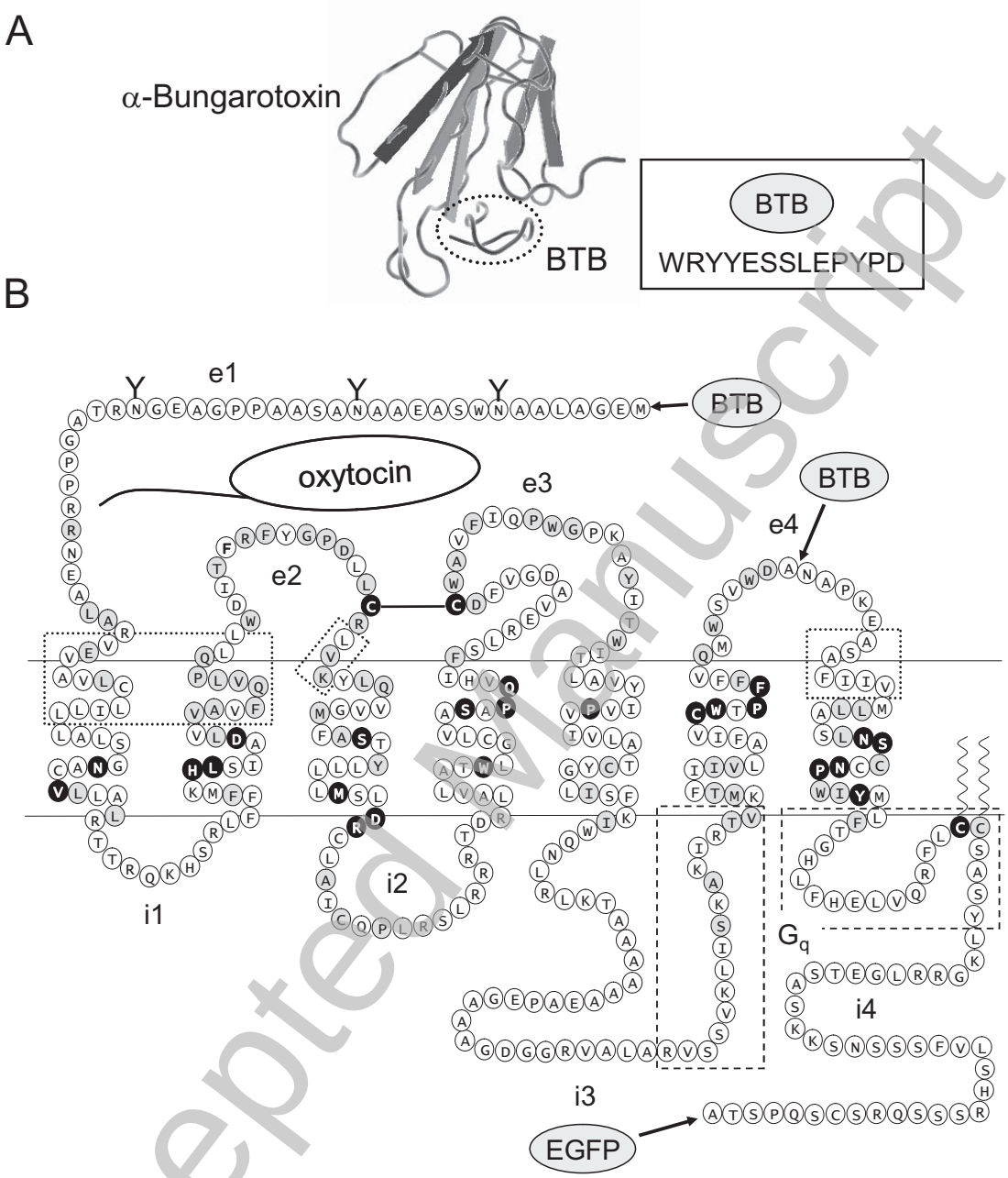

Biochemical Journal Immediate Publication. Published on 12 May 2011 as manuscript BJ20101795

Fig. 2

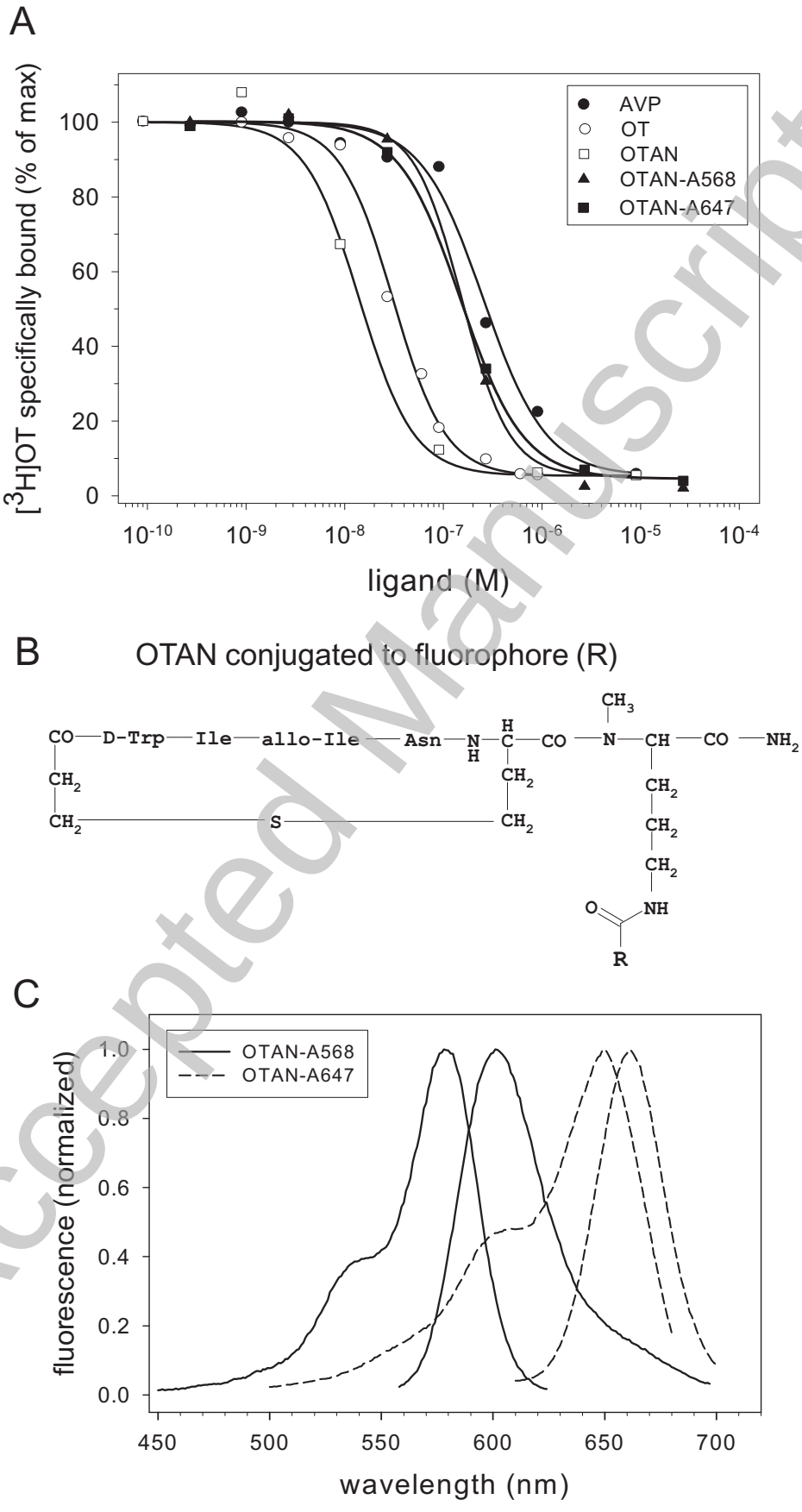

Biochemical Journal Immediate Publication. Published on 12 May 2011 as manuscript BJ20101795

Fig. 3

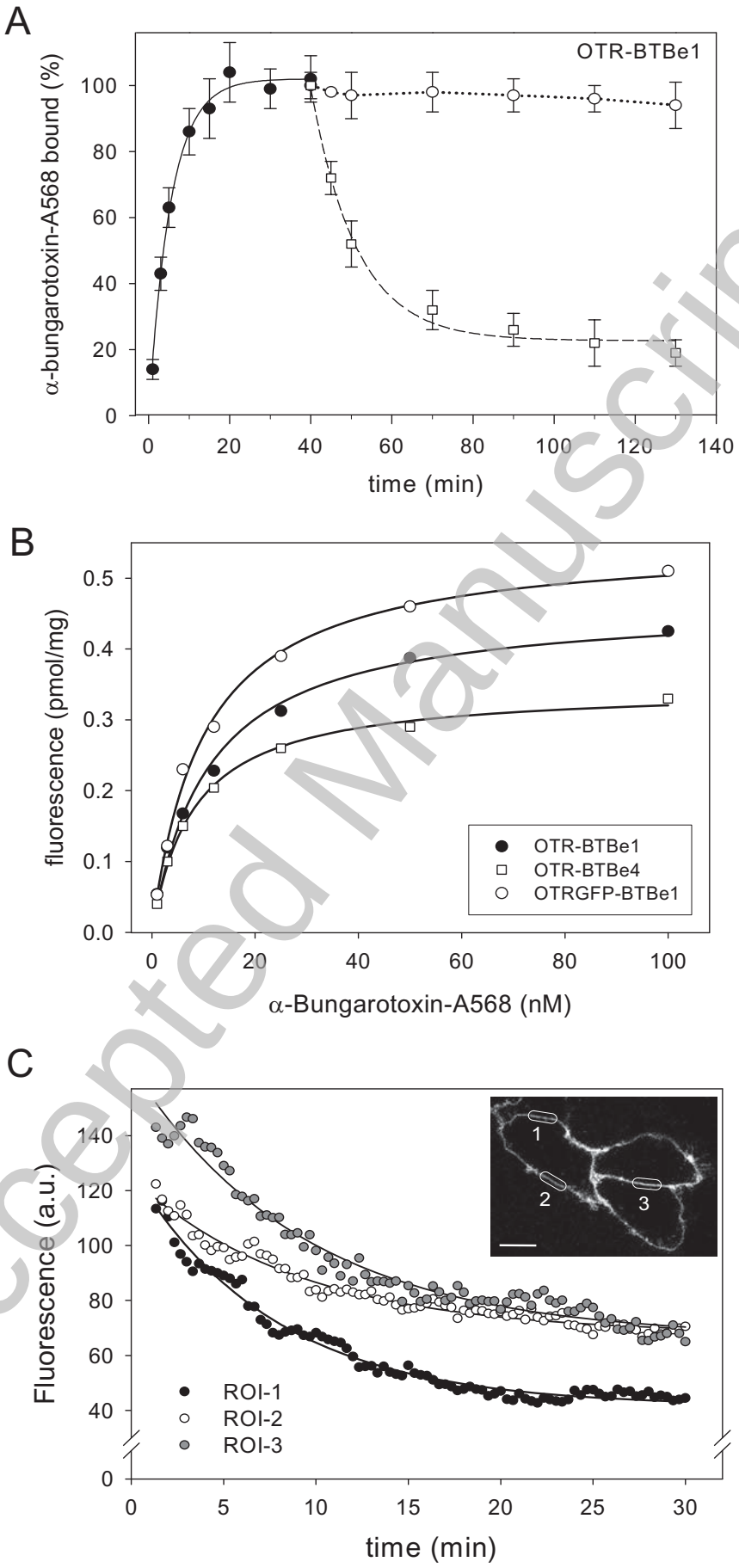

Biochemical Journal Immediate Publication. Published on 12 May 2011 as manuscript BJ20101795

Fig. 4

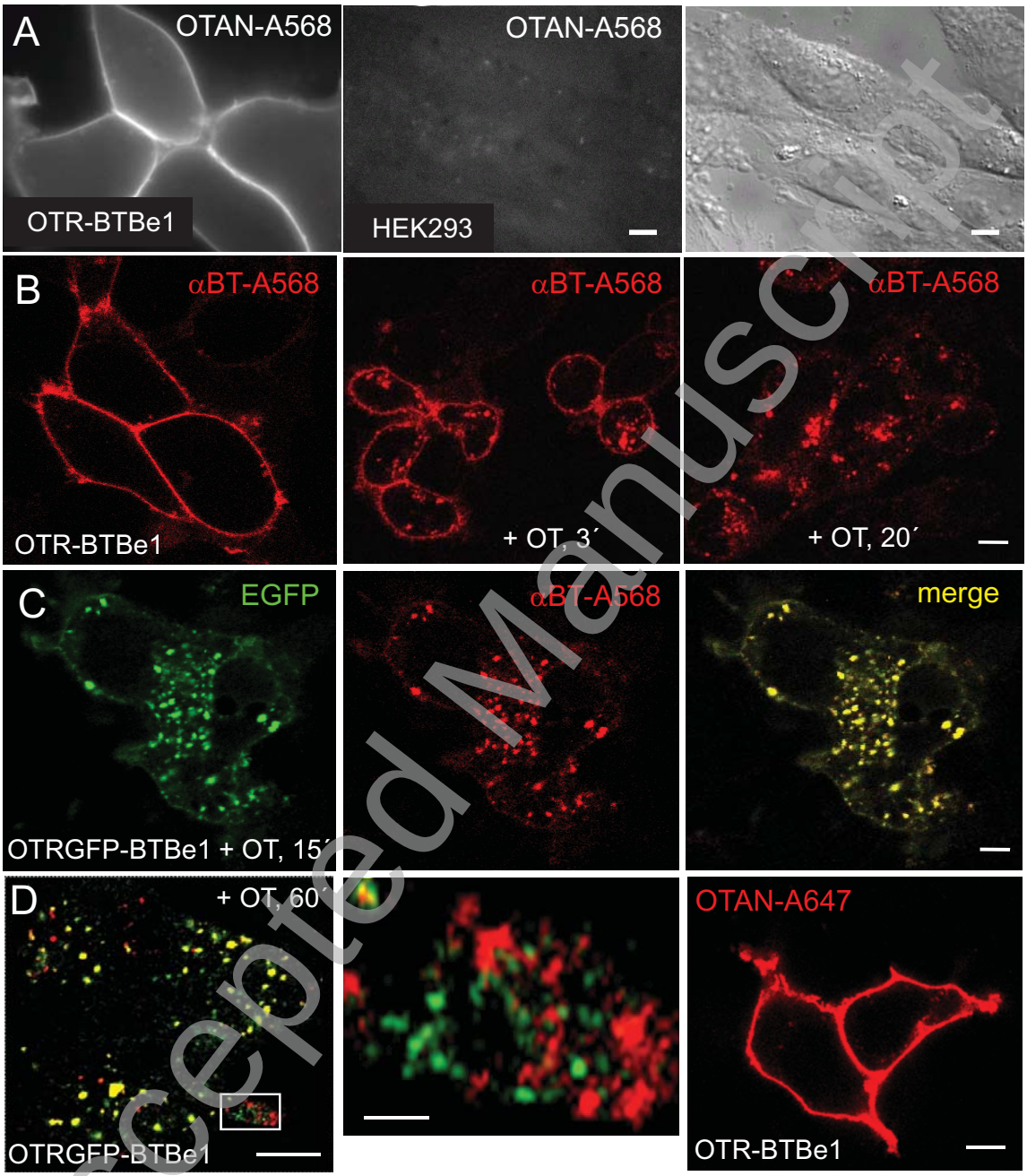

Biochemical Journal Immediate Publication. Published on 12 May 2011 as manuscript BJ20101795

Fig. 5

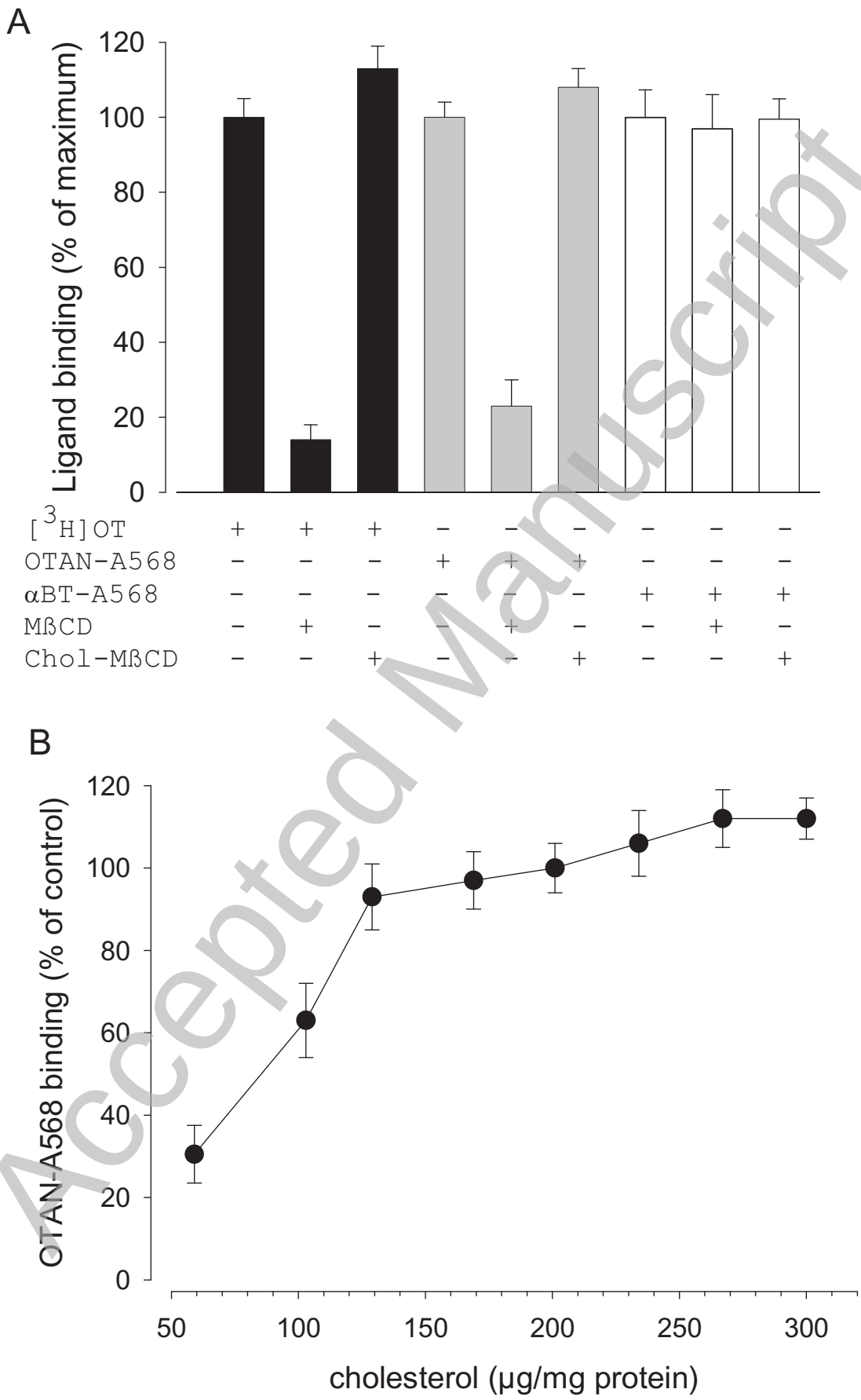

Biochemical Journal Immediate Publication. Published on 12 May 2011 as manuscript BJ20101795

Fig. 6

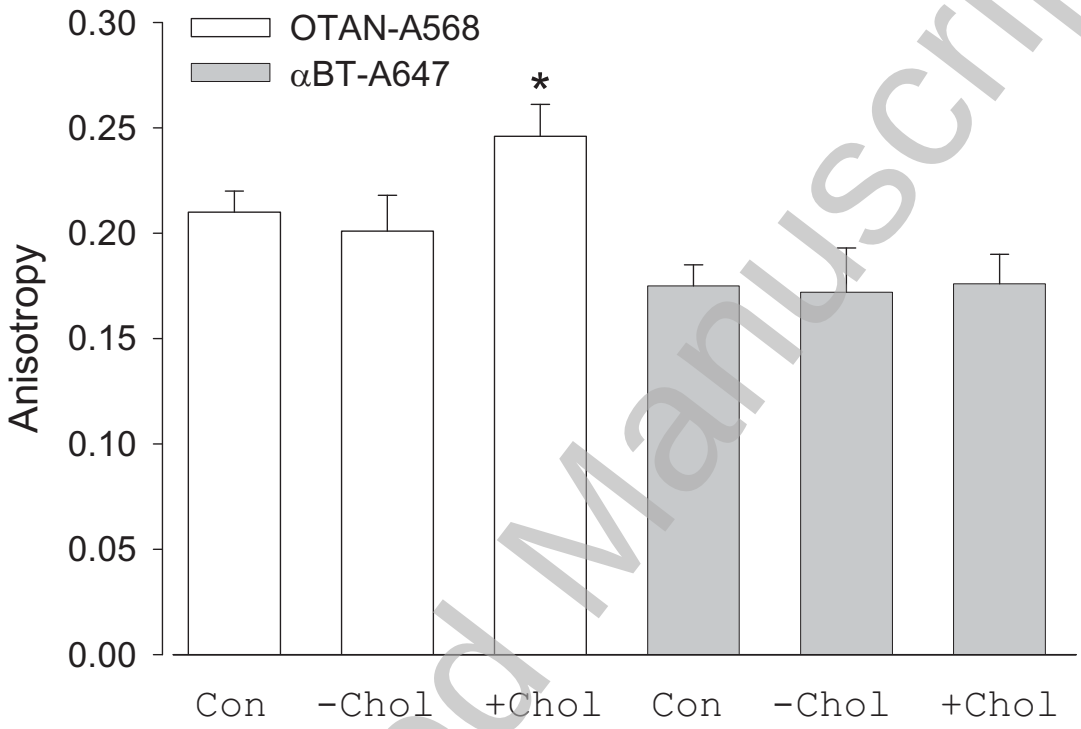

Biochemical Journal Immediate Publication. Published on 12 May 2011 as manuscript BJ20101795

Fig. 7

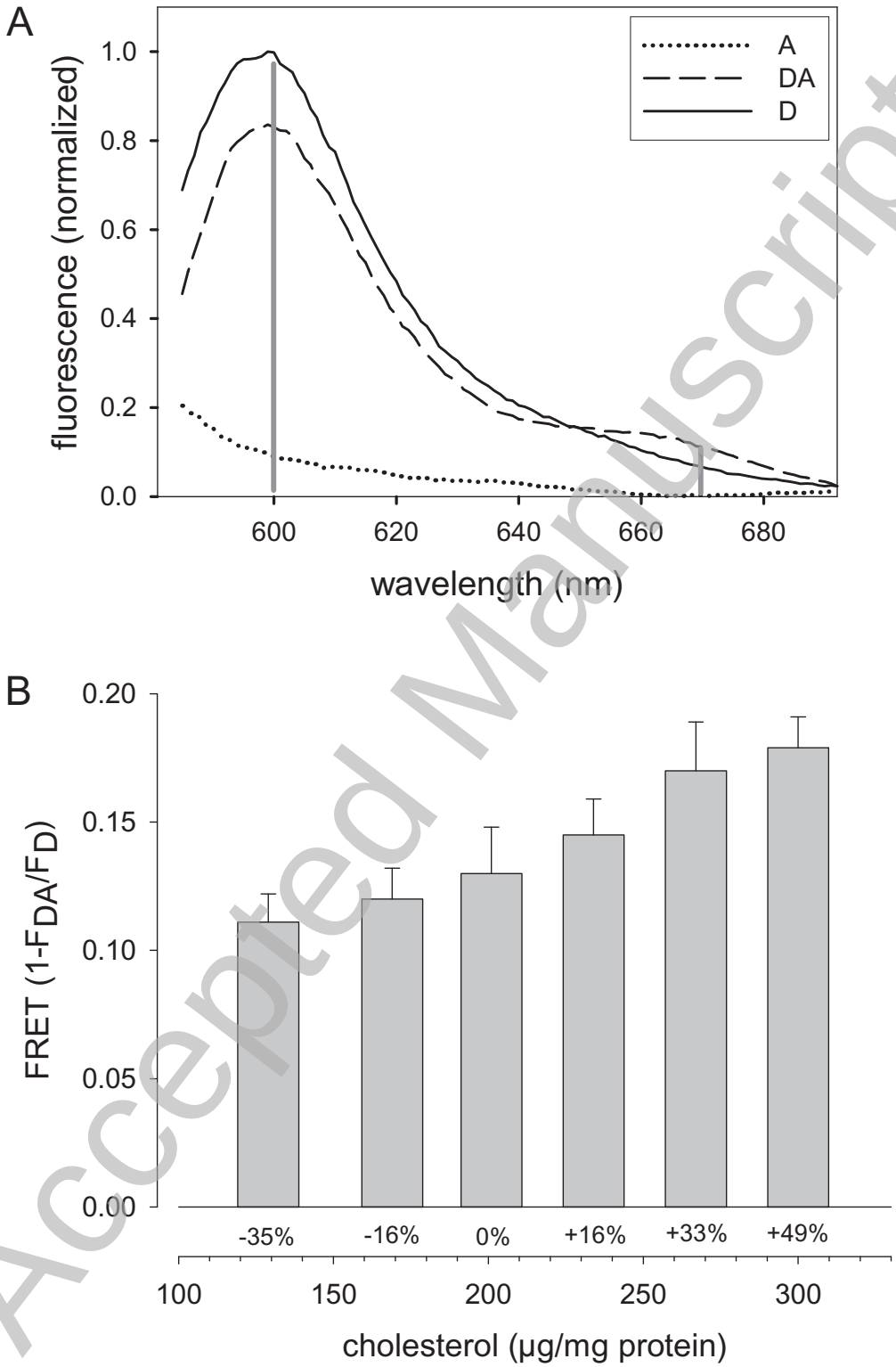

Biochemical Journal Immediate Publication. Published on 12 May 2011 as manuscript BJ20101795

Fig. 8